國立臺灣大學工學院化學工程學系

碩士論文

Department of Chemical Engineering

College of Engineering

National Taiwan University

Master's Thesis

球形複合粒子在非同心球形孔洞中之緩慢移動及轉動

Slow translation and rotation of a composite sphere within a nonconcentric spherical cavity

陳奕銓

Yi-Chuan Chen

指導教授：葛煥彰 教授

Advisor: Huan-Jang Keh, Professor

中華民國 一百一十四 年 七 月

July 2025

doi:10.6342/NTU202502609

國立臺灣大學碩士學位論文
口試委員會審定書

MASTER'S THESIS ACCEPTANCE CERTIFICATE
NATIONAL TAIWAN UNIVERSITY

球形複合粒子在非同心球形孔洞中之緩慢移動及轉動

Slow translation and rotation of a composite sphere within a nonconcentric spherical cavity

本論文係 陳奕銓 （R12524072）在國立臺灣大學 化學工程 （系/所/學位學程）完成之碩(博)士學位論文，於民國 114 年 7 月 16 日承下列考試委員審查通過及口試及格，特此證明。

The undersigned, appointed by the Department / Graduate Institute of chemical engineering on 16/ 07/ 2025 have examined a Master's Thesis entitled above presented by Chen, Yi-Chuan (R12524072) candidate and hereby certify that it is worthy of acceptance.

口試委員 Oral examination committee:

萬煥彰　　謝子賢

（指導教授 Advisor）

詹正雄

系（所、學位學程）主管 Director: 廖英志

doi:10.6342/NTU202502609

謝辭

碩士班期間能夠順利完成這篇論文，要歸功於在臺大就學時遇到的每一位貴人。首先，我由衷感謝葛煥彰教授，在埋首研究的過程中，教授時常關心我們的研究狀況，並提供許多指導與建議，也會在我們遇到困難時，不吝於分享自身見解與過往經驗，教授熱忱的教學精神以及嚴謹踏實的研究態度，更是令我深受啟發。感謝教授這兩年來的教誨與辛勞，以及對我們的信任，讓我在學業及個性上皆成長許多；另外，我也要感謝口試委員詹正雄教授與謝子賢博士，感謝兩位撥冗參與口試，並提供我許多寶貴建議，這些都將成為我未來努力的方向。

接著，我要感謝實驗室的學長姐展維、家菶及永捷，在我剛踏入實驗室時，便熱心解答我對研究的各種疑問，也帶領我逐漸適應校園與生活環境；同時，我也要感謝碩士班期間的同學威鋅及郁富，感謝你們除了研究與課業方面的幫助外，更陪我度過一段充實且歡樂的碩班時光；此外，也感謝學弟陳沂與威齊，讓實驗室始終保持熱絡的氛圍。在此誠摯祝福各位未來一切順利。

最後，我要感謝我的家人，特別是我的父母。感謝你們一路以來的照顧與支持，讓我得以專注於學業無後顧之憂，正因為有你們在背後默默付出，我才能順利完成碩士學業。你們永遠是我最堅強的後盾，我愛你們!

民國 一百一十四年 七月

陳奕銓

doi:10.6342/NTU202502609

摘要

本研究以半解析方式探討一個複合球形粒子(由一實心硬核外部包覆可穿透之多孔層所組成)在一個充滿黏性流體之球形孔洞中，於非同心位置沿其垂直連心方向，所進行的擬穩態低雷諾數移動及轉動。多孔層內外之流體速度分布分別由 Brinkman 方程式及 Stokes 方程式主導，其中粒子外部流體的速度表示式為以粒子中心及孔洞中心為原點的球座標系統之通解組合而成。對於滿足孔洞表面及多孔層內外表面的邊界條件所得之方程組，本研究將透過邊界取點法數值求解，計算出流體施加於粒子之阻力及力矩，且數值解在不同參數組合下均呈現良好收斂性。從計算結果可得複合粒子移動、轉動時所受拖曳力及力矩與粒子結構(如多孔層的厚度及流體穿透度)、粒子在孔洞中的相對位置及大小之關係。流體施加於複合粒子之拖曳力和力矩會隨多孔層穿透度下降、實心硬核對粒子半徑比值增加以及粒子對孔洞半徑比值增加而呈現單調遞增。粒子所受拖曳力和力矩大致上亦會隨其偏心程度增加而遞增。此外，孔洞對於複合粒子移動時的阻礙影響會相較於相同粒子轉動時所受影響更為顯著。複合粒子在孔洞中移動伴隨轉動之耦合效應較為複雜，且並非為粒子對孔洞半徑比值之單調函數。

關鍵詞: 複合粒子、球形孔洞、拖曳力和力矩、蠕動流，多孔粒子

doi:10.6342/NTU202502609

Abstract

A semi-analytical study of coupled translation and rotation of a composite spherical particle (a hard sphere core coated with a permeable porous layer) in a viscous fluid inside an eccentric spherical cavity normal to their common diameter is presented in the quasi-steady limit of low Reynolds number. To solve the Stokes and Brinkman equations for the flow fields outside and inside the porous layer, respectively, a general solution is constructed from the fundamental solutions in the two spherical coordinate systems based on both the composite particle and the cavity. The boundary conditions at the cavity wall and inner and outer surfaces of the porous layer are satisfied by a collocation method. Numerical results for the force and torque exerted on the particle by the fluid are obtained with good convergence for various values of the relevant parameters in practical applications. For the translation and rotation of a composite sphere inside a concentric cavity, our force and torque results agree well with the available solutions in the literature. The force and torque on a translating and rotating particle increase monotonically with increases in the ratios of particle radius to porous layer permeation length, core-to-particle radii, and particle-to-cavity radii. In general, they also increase with an increase in the relative distance between the particle and cavity centers. The boundary effect of the cavity

doi:10.6342/NTU202502609

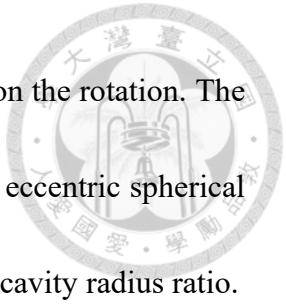

on the translation of the particle is much more pronounced than that on the rotation. The coupling effect in the simultaneous translation and rotation inside an eccentric spherical cavity is complicated and not a monotonic function of the particle-to-cavity radius ratio.

Keywords: composite particle, spherical cavity, drag force and torque, creeping flow, porous sphere

doi:10.6342/NTU202502609

Table of Contents

doi:10.6342/NTU202502609

doi:10.6342/NTU202502609

List of Figures

doi:10.6342/NTU202502609

doi:10.6342/NTU202502609

List of Tables

doi:10.6342/NTU202502609

Chapter 1

Introduction

The low-Reynolds-number translational and rotational motions of small particles in Newtonian fluids continue to be of considerable interest to researchers in various fields of science, technology, and engineering. They are fundamental in nature, but allow one to develop rational understanding of numerous practical systems such as sedimentation, centrifugation, flocculation, filtration, microfluidics, electrophoresis and other phoretic motions. Analysis of this topic was first carried out by Stokes (1845, 1851) for the creeping motions of an unbounded fluid around a translating and rotating hard (impermeable) sphere and later extended to the translation and rotation of composite spheres (Masliyah *et al* 1987, Keh and Chou 2004).

A composite sphere of radius b is a particle with a hard sphere core of radius a coated with a porous (permeable) layer of thickness $b-a$. Typical examples of a composite particle are a polystyrene latex with a porous layer extending from the bulk particle into the fluid (Anderson and Solomentsev 1996) and a biological cell with rough surface appendages ranging from micron-sized cilia to nanometer-sized protein molecules (Wunderlich 1982). The particles in a colloidal suspension can be sterically stabilized

doi:10.6342/NTU202502609

against flocculation by deliberately adsorbing polymers and forming permeable layers (Napper 1983).

The force and torque exerted by an unbounded fluid of viscosity η on a composite particle of radius b with a hard core of radius a translating with velocity $\mathbf{U}$ and rotating with angular velocity $\mathbf{\Omega}$ are (Masliyah *et al* 1987, Keh and Chou 2004)

$$\begin{aligned}\mathbf{F}_0 = -6\pi\eta\lambda^{-1}\mathbf{U}\{&W\lambda a\cosh\lambda a - 3\lambda^2a^2(V+\lambda a\sinh\lambda a)\\&+\cosh(\lambda b-\lambda a)[W(\lambda aV-\lambda b\cosh\lambda a)+3\lambda^3a^2b\sinh\lambda a]\\&+\sinh(\lambda b-\lambda a)[W\cosh\lambda a+3\lambda^2a^2(\lambda aV-\sinh\lambda a)]\}\{(\lambda a\sinh\lambda b\\&-\cosh\lambda a)[(W+3\lambda b)\cosh(\lambda b-\lambda a)+3(\lambda^2a^2-1)\sinh(\lambda b-\lambda a)-6\lambda a]\}^{-1},\end{aligned} \quad (1)$$

$$\mathbf{T}_0 = -8\pi\eta b^3\mathbf{\Omega}\left[1+\frac{3}{\lambda^2b^2}-\frac{3}{\lambda b}\frac{\cosh(\lambda b-\lambda a)+\lambda a\sinh(\lambda b-\lambda a)}{\sinh(\lambda b-\lambda a)+\lambda a\cosh(\lambda b-\lambda a)}\right], \quad (2)$$

respectively, where

$$V = \lambda b\sinh\lambda b-\cosh\lambda b, \quad (3a)$$

$$W = 2\lambda^3b^3+\lambda^3a^3+3\lambda a, \quad (3b)$$

and λ^{-1} is the flow penetration length or square root of the fluid permeability in the porous surface layer of the particle. Note that the translation and rotation of the unconfined composite sphere are not coupled with each other; i.e., $\mathbf{F}_0$ and $\mathbf{T}_0$ are not related with $\mathbf{\Omega}$ and $\mathbf{U}$, respectively. In the limiting cases of $a=b$ and $a=0$, equations (1) and (2) degenerate to the Stokes results ($\mathbf{F}_0 = 6\pi\eta b\mathbf{U}$ and $\mathbf{T}_0 = 8\pi\eta b^3\mathbf{\Omega}$)

doi:10.6342/NTU202502609

of a hard sphere and corresponding results of a completely permeable (porous) sphere (Neale *et al* 1973, Keh and Chou 2004), respectively, of radius b. In the limits $\lambda b = 0$ and $\lambda b \to \infty$, these equations reduce to the Stokes results of a hard sphere of radius a and radius b, respectively.

In the real case of creeping motions, particles are not isolated and the ambient fluid is restricted by solid boundaries (Happel and Brenner 1983, Malysa and van de Ven 1986, Anderson 1989, Romanò *et al* 2020). Therefore, it is necessary to determine whether the presence of a neighboring boundary significantly affects the motions of the particles. The low-Reynolds-number translational and rotational motions of a hard sphere confined by adjacent boundaries, such as inside a spherical cavity (Keh and Chang 1998, Keh and Lee 2010, Lee and Keh 2013a, Papavassiliou and Alexander 2017, Chou and Keh 2021), in a circular cylinder (Brenner and Sonshine 1964, Bungay and Brenner 1973, Greenstein and Schiavina 1975, Leichtberg *et al* 1976, Keh and Chang 2007, Lee and Keh 2021), and near one or two planes (Brenner 1961, Dean and O'Neill 1963, Goldman *et al* 1967, Ganatos *et al* 1980a,b, Chen and Keh 2003, Chang and Keh 2006, Liao and Keh 2022), were examined extensively. In the same way, the slow translation and rotation of a composite sphere within a concentric spherical cavity (Keh and Chou 2004, Srinivasacharya and Krishna Prasad 2012, Prakash and Raja Sekhar 2017), in a circular cylinder (Jhuang and Keh 2022), and normal to one or two planes (Anderson and

doi:10.6342/NTU202502609

Solomentsev 1996, Chen and Ye 2000, Chang and Keh 2023), as well as an entirely porous sphere within an eccentric spherical cavity (Saad 2016, Sherief *et al* 2016, Krishna Prasad 2021), were also analyzed. Recently, the axisymmetric translation (as given in Appendix B) and rotation (Chou and Keh 2022) of a composite sphere within an eccentric spherical cavity have been analytically studied. These investigations indicate that the boundary effect on the motions of hard, porous, and composite particles can be important and interesting.

The purpose of the main text of this thesis is to obtain a semi-analytical solution for the slow translation and rotation of a composite sphere in a nonconcentric spherical cavity normal to their common diameter. This normal motion is more difficult to handle mathematically because the azimuthal symmetry is broken. The Stokes and Brinkman equations for the external and internal flow fields, respectively, of the porous layer are solved by using a combination of analytical and numerical methods with a boundary collocation technique, and the wall-corrected drag force and torque exerted by the fluid on the particle are obtained with good convergence. Since the general problem of translation and rotation of a composite sphere in arbitrary directions inside an eccentric spherical cavity is linear, its solution can be obtained by the superposition of solutions to its two subproblems: motions along/about their common diameter, which was previously examined (Chou and Keh 2022, Appendix B), and motions perpendicular to their

doi:10.6342/NTU202502609

common diameter, which is treated in the main text of this thesis.

doi:10.6342/NTU202502609

Chapter 2

Analysis

We consider the creeping flow caused by a spherical composite particle of radius b, composed of a rigid sphere core of radius a and a porous surface layer of thickness $b-a$, translating with a velocity $\mathbf{U}=U\mathbf{e}_x$ and rotating with an angular velocity $\mathbf{\Omega}=\Omega\mathbf{e}_y$ in an incompressible Newtonian fluid of viscosity η inside a nonconcentric spherical cavity of radius c, as shown in figure 1, in quasi-steady state. Here, (x,y,z), (ρ,ϕ,z), and (r_2,θ_2,ϕ) represent the rectangular, circular cylindrical, and spherical coordinate systems, respectively, originating from the cavity center; (r_1,θ_1,ϕ) denotes the spherical coordinate system originating from the particle center; $\mathbf{e}_x$ and $\mathbf{e}_y$ are the unit vectors in the x and y directions, respectively. The particle center is instantaneously situated away from the cavity center at a distance d in the z direction (coinciding with the particle-and-cavity common diameter). The objective is to determine the correction to equations (1) and (2) for the translation and rotation of the composite sphere due to the presence of the cavity wall.

doi:10.6342/NTU202502609

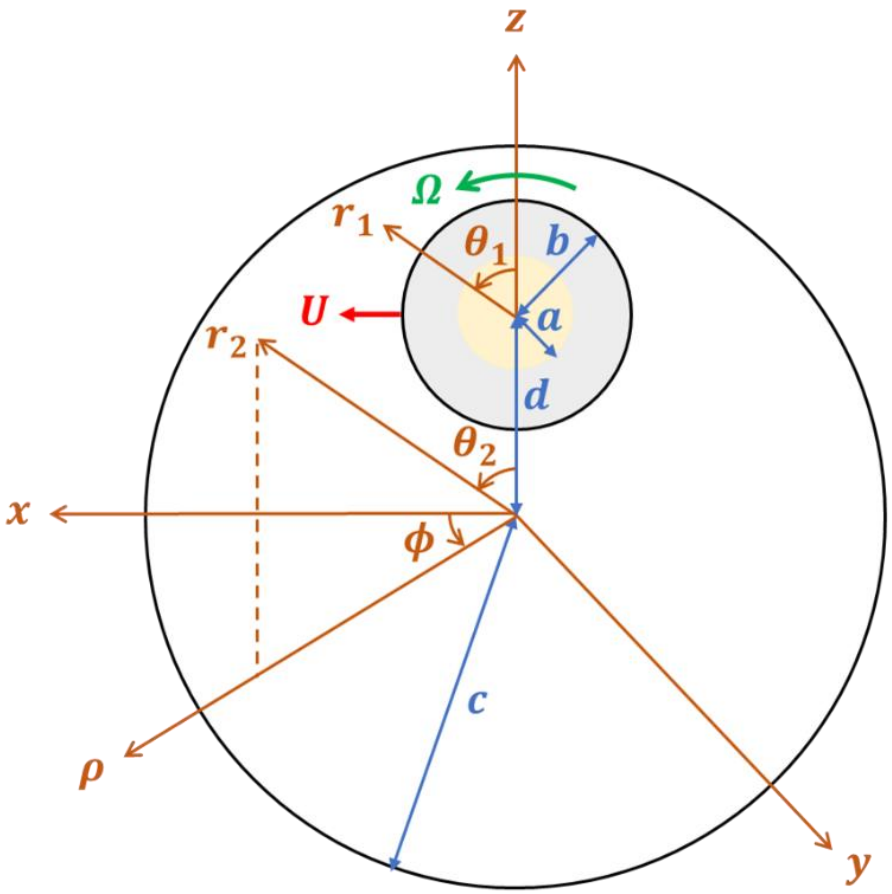

Figure 1 Geometrical sketch of the translation and rotation of a composite sphere in an eccentric spherical cavity perpendicular to their common diameter.

doi:10.6342/NTU202502609

2.1 Governing equations and boundary conditions

The fluid motions outside the composite particle and inside its porous surface layer are governed by the Stokes and Brinkman equations, respectively:

$$\eta\nabla^2\mathbf{v}-\nabla p=\mathbf{0}, \qquad \nabla\cdot\mathbf{v}=0 \qquad (r_1\geq b \text{ and } r_2\leq c), \tag{4}$$

$$\eta\nabla^2\hat{\mathbf{v}}-\eta\lambda^2(\hat{\mathbf{v}}-U\mathbf{e}_x-\Omega\mathbf{e}_y\times r_1\mathbf{e}_{r1})-\nabla\hat{p}=\mathbf{0}, \qquad \nabla\cdot\hat{\mathbf{v}}=0 \qquad (a\leq r_1\leq b). \tag{5}$$

Here $\mathbf{v}$ and $\hat{\mathbf{v}}$ are the fluid velocity fields for the external (outside the particle) and internal (inside the porous layer) flows, respectively, p and $\hat{p}$ are the corresponding dynamic pressure distributions, and $\mathbf{e}_{ri}$ together with $\mathbf{e}_{\theta i}$ and $\mathbf{e}_{\phi}$ are the basic unit vectors in the spherical coordinate system (r_i,θ_i,ϕ).

The boundary conditions for the fluid flows are

$$r_1=a: \qquad \hat{\mathbf{v}}=U\mathbf{e}_x+a\Omega\mathbf{e}_y\times\mathbf{e}_{r1}, \tag{6}$$

$$r_1=b: \qquad \mathbf{v}=\hat{\mathbf{v}}, \tag{7a}$$

$$\mathbf{e}_{r1}\cdot(\boldsymbol{\tau}-p\mathbf{I})=\mathbf{e}_{r1}\cdot(\hat{\boldsymbol{\tau}}-\hat{p}\mathbf{I}), \tag{7b}$$

$$r_2=c: \qquad \mathbf{v}=\mathbf{0}. \tag{8}$$

Here, $\boldsymbol{\tau}=\eta[\nabla\mathbf{v}+(\nabla\mathbf{v})^{\mathrm{T}}]$ and $\hat{\boldsymbol{\tau}}=\eta[\nabla\hat{\mathbf{v}}+(\nabla\hat{\mathbf{v}})^{\mathrm{T}}]$ are the deviatoric stress tensors for the external and internal flows, respectively, and $\mathbf{I}$ is the unit dyadic.

doi:10.6342/NTU202502609

2.2 General solutions for external and internal fluid velocities

Since the governing equations and boundary conditions are linear, the velocity field $\mathbf{v}$ and pressure p outside the particle can be decomposed into two parts (Lee and Keh 2013a),

$$\mathbf{v} = \mathbf{v}_1 + \mathbf{v}_2, \qquad p = p_1 + p_2, \tag{9}$$

where $\mathbf{v}_i$ and p_i are the solution of equation (4) in spherical coordinate system (r_i, θ_i, ϕ) with

$$\mathbf{v}_i = v_{ir}\mathbf{e}_{ri} + v_{i\theta}\mathbf{e}_{\theta i} + v_{i\phi}\mathbf{e}_{\phi}, \qquad i = 1, 2. \tag{10}$$

The velocity $\mathbf{v}_1$ and pressure p_1 represent the disturbances generated by the particle with Lamb's general solution (Happel and Brenner 1983)

$$v_{1r} = \sum_{n=1}^{\infty}(n+1)(C_{1n}r_1^{-n-2} + A_{1n}r_1^{-n})P_n^1(\mu_1)\cos\phi, \tag{11a}$$

$$v_{1\theta} = \sum_{n=1}^{\infty}[B_{1n}r_1^{-n-1}P_n^1(\mu_1)(1-\mu_1^2)^{-1/2} + (C_{1n}r_1^{-n-2} + A_{1n}\frac{n-2}{n}r_1^{-n})\frac{\mathrm{d}P_n^1(\mu_1)}{\mathrm{d}\mu_1}(1-\mu_1^2)^{1/2}]\cos\phi, \tag{11b}$$

$$v_{1\phi} = \sum_{n=1}^{\infty}[B_{1n}r_1^{-n-1}\frac{\mathrm{d}P_n^1(\mu_1)}{\mathrm{d}\mu_1}(1-\mu_1^2)^{1/2} + (C_{1n}r_1^{-n-2} + A_{1n}\frac{n-2}{n}r_1^{-n})P_n^1(\mu_1)(1-\mu_1^2)^{-1/2}]\sin\phi, \tag{11c}$$

$$p_1 = 2\eta\sum_{n=1}^{\infty}A_{1n}(2n-1)r_1^{-n-1}P_n^1(\mu_1)\cos\phi, \tag{11d}$$

doi:10.6342/NTU202502609

whereas $\mathbf{v}_2$ and p_2 denote the disturbances produced by the cavity wall with

$$v_{2r} = \sum_{n=1}^{\infty} n(C_{2n} r_2^{n-1} + A_{2n} r_2^{n+1}) P_n^1(\mu_2)\cos\phi\,, \tag{12a}$$

$$v_{2\theta} = \sum_{n=1}^{\infty} [B_{2n} r_2^{n} P_n^1(\mu_2)(1-\mu_2^2)^{-1/2}$$

$$-(C_{2n} r_2^{n-1} + A_{2n}\frac{n+3}{n+1} r_2^{n+1})\frac{\mathrm{d}P_n^1(\mu_2)}{\mathrm{d}\mu_2}(1-\mu_2^2)^{1/2}]\cos\phi\,, \tag{12b}$$

$$v_{2\phi} = \sum_{n=1}^{\infty} [B_{2n} r_2^{n} \frac{\mathrm{d}P_n^1(\mu_2)}{\mathrm{d}\mu_2}(1-\mu_2^2)^{1/2}$$

$$-(C_{2n} r_2^{n-1} + A_{2n}\frac{n+3}{n+1} r_2^{n+1}) P_n^1(\mu_2)(1-\mu_2^2)^{-1/2}]\sin\phi\,, \tag{12c}$$

$$p_2 = 2\eta \sum_{n=1}^{\infty} A_{2n}(2n+3) r_2^{n} P_n^1(\mu_2)\cos\phi\,. \tag{12d}$$

In the previous equations, P_n^1 are the associated Legendre Polynomials, $\mu_i = \cos\theta_i$, and the unknown constants A_{in}, B_{in}, and C_{in} need to be determined.

The velocity field $\hat{\mathbf{v}}$ and pressure $\hat{p}$ inside the porous surface layer of the composite particle can be expressed as (Sherief *et al* 2016)

$$\hat{\mathbf{v}} = \hat{v}_r \mathbf{e}_{r1} + \hat{v}_\theta \mathbf{e}_{\theta 1} + \hat{v}_\phi \mathbf{e}_\phi\,, \tag{13}$$

$$\hat{v}_r = U(1-\mu_1^2)^{1/2}\cos\phi + \sum_{n=1}^{\infty} n(n+1)\{\hat{C}_{2n} r_1^{n-1} + \hat{C}_{1n} r_1^{-n-2}$$

$$+\lambda^{-1/2} r_1^{-3/2}[\hat{A}_{2n} I_{n+1/2}(\lambda r_1) + \hat{A}_{1n} K_{n+1/2}(\lambda r_1)]\} P_n^1(\mu_1)\cos\phi\,, \tag{14a}$$

$$\hat{v}_\theta = (U\mu_1 + r_1\Omega)\cos\phi + \sum_{n=1}^{\infty}\{(\lambda r_1)^{-1/2}[\hat{B}_{2n} I_{n+1/2}(\lambda r_1) + \hat{B}_{1n} K_{n+1/2}(\lambda r_1)] P_n^1(\mu_1)(1-\mu_1^2)^{-1/2}$$

$$+[\hat{C}_{2n}(-n-1) r_1^{n-1} + \hat{C}_{1n} n r_1^{-n-2} + \lambda^{-1/2} r_1^{-3/2}\{\hat{A}_{2n}[n I_{n+1/2}(\lambda r_1) - \lambda r_1 I_{n-1/2}(\lambda r_1)]$$

doi:10.6342/NTU202502609

$$+\hat{A}_{1n}[nK_{n+1/2}(\lambda r_1)+\lambda r_1 K_{n-1/2}(\lambda r_1)]\}]\frac{\mathrm{d}P_n^1(\mu_1)}{\mathrm{d}\mu_1}(1-\mu_1^{\,2})^{1/2}\}\cos\phi\,, \tag{14b}$$

$$\hat{v}_\phi = -(U+r_1\Omega\mu_1)\sin\phi+\sum_{n=1}^{\infty}\{(\lambda r_1)^{-1/2}[\hat{B}_{2n}I_{n+1/2}(\lambda r_1)+\hat{B}_{1n}K_{n+1/2}(\lambda r_1)]\frac{\mathrm{d}P_n^1(\mu_1)}{\mathrm{d}\mu_1}(1-\mu_1^{\,2})^{1/2}$$

$$+[\hat{C}_{2n}(-n-1)r_1^{n-1}+\hat{C}_{1n}nr_1^{-n-2}+\lambda^{-1/2}r_1^{-3/2}\{\hat{A}_{2n}[nI_{n+1/2}(\lambda r_1)-\lambda r_1 I_{n-1/2}(\lambda r_1)]$$

$$+\hat{A}_{1n}[nK_{n+1/2}(\lambda r_1)+\lambda r_1 K_{n-1/2}(\lambda r_1)]\}]P_n^1(\mu_1)(1-\mu_1^{\,2})^{-1/2}\}\sin\phi\,, \tag{14c}$$

$$\hat{p}=\eta\lambda^2\sum_{n=1}^{\infty}[\hat{C}_{2n}(-n-1)r_1^{\,n}+\hat{C}_{1n}nr_1^{-n-1}]P_n^1(\mu_1)\cos\phi\,, \tag{14d}$$

where I_n and K_n are the modified Bessel functions of the first and second kinds, respectively, and $\hat{A}_{in}$, $\hat{B}_{in}$, and $\hat{C}_{in}$ are unknown constants to be determined. Note that the solutions for $\mathbf{v}$, $\hat{\mathbf{v}}$, p, and $\hat{p}$ are only proportional to either $\cos\phi$ or $\sin\phi$ (and do not contain the higher-order harmonics) due to the axial symmetry of the system geometry.

2.3 Transformation between two spherical coordinate systems

A solution of the form in equations (9)-(14) immediately satisfies the requirement that the velocity is finite for any position in the fluid phases. In order to express these equations with a single spherical coordinate system, coordinate transformation is required. The coordinates r_2 and μ_2 of any position are related to the coordinates r_1 and μ_1 of that position through the following formulas:

$$r_2=[r_1^2(1-\mu_1^{\,2})+(r_1\mu_1+d)^2]^{1/2}\,,\qquad \mu_2=(r_1\mu_1+d)/r_2\,. \tag{15}$$

doi:10.6342/NTU202502609

The relationship between the principal unit vectors of the two coordinate systems is

$$\mathbf{e}_{r2} = f^{(1)}\mathbf{e}_{r1} + f^{(2)}\mathbf{e}_{\theta 1}, \qquad \mathbf{e}_{\theta 2} = f^{(1)}\mathbf{e}_{\theta 1} - f^{(2)}\mathbf{e}_{r1}, \tag{16}$$

where

$$f^{(1)} = (1-\mu_2{}^2)^{1/2}(1-\mu_1{}^2)^{1/2} + \mu_1\mu_2, \tag{17a}$$

$$f^{(2)} = (1-\mu_2{}^2)^{1/2}\mu_1 - (1-\mu_1{}^2)^{1/2}\mu_2 . \tag{17b}$$

Applying the boundary conditions at the inner and outer surfaces of the porous layer of the composite particle and cavity wall given by equations (6)-(8) to equations (9)-(14), we obtain equations (A1)-(A12), which are lengthy, in Appendix A. The unknown constants $\hat{A}_{in}$, $\hat{B}_{in}$, $\hat{C}_{in}$, A_{in}, B_{in}, and C_{in} with $i=1$ and 2 are to be determined using these lengthy equations.

2.4 Numerical method

A check of equations (A1)-(A12) shows that the solution to the resulting coefficient matrix is independent of the ϕ coordinate of the boundary points on the spherical surfaces $r_1 = a$, $r_1 = b$ and $r_2 = c$. To satisfy these conditions exactly along the entire surfaces of the porous layer and cavity wall would require the solution to the whole infinite array of the unknown constants A_{in}, B_{in}, C_{in}, $\hat{A}_{in}$, $\hat{B}_{in}$, and $\hat{C}_{in}$ with $i=1$ and 2. However, the collocation technique (Lee and Keh 2013a) enforces the boundary conditions at a finite number of discrete points on the half-circular generating arc

doi:10.6342/NTU202502609

(longitude with θ_j from 0 to π) of each of the spherical surface and truncates the infinite series in equations (11), (12), and (14) into finite ones. If the spherical boundaries are approximated by satisfying the conditions of equations (6)-(8) at *N* discrete points on each generating arc, these infinite series are truncated after *N* terms, resulting in a system of 12*N* simultaneous linear algebraic equations in the truncated form of equations (A1)-(A12). This matrix equation can be solved to yield the 12*N* unknown constants A_{in}, B_{in}, C_{in}, $\hat{A}_{in}$, $\hat{B}_{in}$, and $\hat{C}_{in}$ appearing in the truncated form of equations (11), (12), and (14). The fluid velocity field is completely obtained once these coefficients are solved for a sufficiently large value of *N*.

2.5 Hydrodynamic force and torque on composite sphere

The hydrodynamic drag force $\mathbf{F} = F\mathbf{e}_x$ and torque $\mathbf{T} = T\mathbf{e}_y$ acting on the composite sphere can be calculated by integrations involving the total fluid stress (combination of viscous stress and pressure) over the particle surface, with the result

$$F = 8\pi\eta A_{11}, \tag{18}$$

$$T = 8\pi\eta B_{11}. \tag{19}$$

These expressions show that only the lowest-order coefficients A_{11} and B_{11} contribute to the force and torque. As $b/(c-d) = 0$, the cavity wall is infinitely far from the particle

doi:10.6342/NTU202502609

and equations (18) and (19) reduce to equations (1) and (2) for the translational and rotational motions of an unconfined composite sphere.

The force and torque in equations (18) and (19) can be related to the translational and angular velocities of the composite sphere by

$$F = \frac{F_0}{U}(F_t U + F_r b\Omega), \tag{20}$$

$$T = \frac{T_0}{b\Omega}(T_t U + T_r b\Omega), \tag{21}$$

where F_t, F_r, T_t, and T_r are the dimensionless resistance coefficients calculated using constants A_{11} and B_{11}. According to the cross-effect theory of the force and torque on the spherical particle (Goldman *et al* 1967), it can be proven that the coupling coefficients F_r and T_t satisfy the relationship

$$T_t = \frac{F_0 / U}{T_0 / b^2\Omega} F_r. \tag{22}$$

Therefore, it is only necessary to give the solutions for the three coefficients F_t, T_r, and F_r (or T_t). Note that the values of F_0 / U and T_0 / Ω in equations (20)-(22) can be calculated using equations (1) and (2).

doi:10.6342/NTU202502609

Chapter 3

Results and Discussion

Results of the force, torque, and coupling coefficients F_t, T_r, and F_r (or T_t) in equations (20) and (21) for the slow translational and rotational motions of a composite sphere inside an eccentric spherical cavity normal to their common diameter, obtained by using the boundary collocation method for numerous values of the ratios of particle radius to porous layer permeation length λb, distance between the centers to radius difference of the particle and cavity $d/(c-b)$, particle-to-cavity radii b/c, and core-to-particle radii a/b, are presented for the special case of porous sphere ($a=0$) in tables 1-3 and for the general case in table 4 (convergent to at least the significant figures as given). In the limiting case of $\lambda b \to \infty$, our solutions agree with the corresponding results (Lee and Keh 2013a) obtained for a hard sphere of radius b translating and rotating in a spherical cavity.

doi:10.6342/NTU202502609

Table 1 The force coefficient F_t for the translation of a porous sphere ($a = 0$) within an eccentric spherical cavity perpendicular to their common diameter with different values of $d/(c-b)$, b/c, and λb.

$\frac{d}{(c-b)}$	b/c	F_t					
		$\lambda b = 0.1$	$\lambda b = 1$	$\lambda b = 10$	$\lambda b = 100$	$\lambda b = 500$	$\lambda b \to \infty$
0.25	0.1	1.00050	1.04141	1.25090	1.28734	1.29033	1.29106
	0.2	1.00098	1.08412	1.63521	1.75509	1.76510	1.76757
	0.3	1.00142	1.12619	2.24472	2.56103	2.58796	2.59460
	0.4	1.00180	1.16552	3.24915	4.05757	4.12795	4.14527
	0.5	1.00211	1.19998	4.96145	7.12527	7.32003	7.36765
	0.6	1.00235	1.22774	7.91293	14.3342	14.9529	15.1016
	0.7	1.00252	1.24767	12.7202	35.0735	37.6291	38.2196
	0.8	1.00262	1.25958	19.0178	117.849	135.862	139.647
	0.9	1.00266	1.26463	23.8937	673.088	1133.79	1222.21
	0.95	1.00266	1.26534	24.8527	1677.67	7859.89	10257.2
	0.99	1.00266	1.26545	25.0230	2235.07	52200.0	1333654
	0.999	1.00266	1.26545	25.0247	2244.98	55659.7	1.35E+09
0.5	0.1	1.00053	1.04395	1.26950	1.30919	1.31243	1.31323
	0.2	1.00102	1.08745	1.67450	1.80500	1.81587	1.81855
	0.3	1.00145	1.12893	2.30684	2.65137	2.68058	2.68778
	0.4	1.00181	1.16694	3.33420	4.21533	4.29176	4.31051
	0.5	1.00211	1.20007	5.05737	7.41248	7.62462	7.67616
	0.6	1.00234	1.22699	7.96856	14.9083	15.5864	15.7477
	0.7	1.00251	1.24676	12.6241	36.3899	39.2250	39.8674
	0.8	1.00261	1.25905	18.7573	121.145	141.521	145.680
	0.9	1.00266	1.26452	23.7699	664.720	1174.17	1275.03
	0.95	1.00266	1.26532	24.8271	1637.55	7910.65	10700.4
	0.99	1.00266	1.26544	25.0226	2233.52	51720.7	1391281
	0.999	1.00266	1.26545	25.0247	2244.98	55658.6	1.40E+09

doi:10.6342/NTU202502609

Table 2 The torque coefficient T_r for the rotation of a porous sphere ($a = 0$) within an eccentric spherical cavity perpendicular to their common diameter with different values of $d/(c-b)$, b/c, and λb.

$\frac{d}{(c-b)}$	b/c	T_r					
		$\lambda b = 0.1$	$\lambda b = 1$	$\lambda b = 10$	$\lambda b = 100$	$\lambda b = 500$	$\lambda b \to \infty$
0.25	0.1	1.00000	1.00008	1.00099	1.00131	1.00134	1.00135
	0.2	1.00001	1.00062	1.00753	1.01006	1.01031	1.01037
	0.3	1.00002	1.00198	1.02466	1.03319	1.03404	1.03425
	0.4	1.00005	1.00447	1.05781	1.07890	1.08103	1.08157
	0.5	1.00009	1.00843	1.11440	1.15985	1.16453	1.16571
	0.6	1.00015	1.01417	1.20654	1.29989	1.30988	1.31241
	0.7	1.00024	1.02209	1.35723	1.55304	1.57550	1.58122
	0.8	1.00034	1.03269	1.61960	2.07447	2.13534	2.15088
	0.9	1.00048	1.04663	2.15295	3.56024	3.84241	3.91569
	0.95	1.00057	1.05514	2.68095	6.10100	7.15071	7.48248
	0.99	1.00064	1.06279	3.42910	17.1988	28.7220	36.0981
	0.999	1.00066	1.06463	3.67393	30.6736	111.831	358.118
0.5	0.1	1.00000	1.00018	1.00223	1.00297	1.00304	1.00306
	0.2	1.00002	1.00118	1.01475	1.01982	1.02032	1.02045
	0.3	1.00004	1.00328	1.04281	1.05843	1.06000	1.06039
	0.4	1.00007	1.00655	1.09061	1.12686	1.13056	1.13150
	0.5	1.00012	1.01106	1.16383	1.23876	1.24662	1.24861
	0.6	1.00018	1.01693	1.27190	1.42158	1.43809	1.44227
	0.7	1.00026	1.02447	1.43288	1.73829	1.77561	1.78498
	0.8	1.00036	1.03425	1.69217	2.36540	2.47014	2.49584
	0.9	1.00050	1.04720	2.20112	4.02012	4.54377	4.67236
	0.95	1.00057	1.05530	2.70534	6.59260	8.39244	9.05476
	0.99	1.00064	1.06280	3.43126	17.5438	30.5998	44.1787
	0.999	1.00066	1.06463	3.67397	30.6927	112.784	439.396

doi:10.6342/NTU202502609

Table 3 The coupling coefficient F_r for the motion of a porous sphere ($a = 0$) within an eccentric spherical cavity perpendicular to their common diameter with different values of $d/(c-b)$, b/c, and λb.

$\frac{d}{(c-b)}$	b/c	$-F_r = -T_t(T_0/b^2\Omega)/(F_0/U)$					
		$\lambda b = 0.1$	$\lambda b = 1$	$\lambda b = 10$	$\lambda b = 100$	$\lambda b = 500$	$\lambda b \to \infty$
0.25	0.1	2.28E-06	0.00022	0.00312	0.00425	0.00437	0.00439
	0.2	7.80E-06	0.00077	0.01382	0.01956	0.02013	0.02028
	0.3	1.44E-05	0.00148	0.03492	0.05209	0.05382	0.05426
	0.4	2.01E-05	0.00214	0.07062	0.11422	0.11866	0.11977
	0.5	2.33E-05	0.00256	0.12630	0.23285	0.24391	0.24667
	0.6	2.28E-05	0.00257	0.20459	0.47346	0.50283	0.51004
	0.7	1.85E-05	0.00214	0.28887	1.02391	1.11690	1.13889
	0.8	1.14E-05	0.00134	0.31039	2.56615	3.00649	3.10125
	0.9	3.83E-06	0.00046	0.17866	7.85163	13.5020	14.6054
	0.95	1.10E-06	0.00013	0.07029	9.84411	47.9625	62.8731
	0.99	4.90E-08	5.98E-06	0.00442	2.05061	62.9921	1661.34
	0.999	6.96E-10	6.15E-08	5.00E-05	0.04770	3.83860	168150
0.5	0.1	4.97E-06	0.00047	0.00688	0.00940	0.00965	0.00971
	0.2	1.63E-05	0.00162	0.02977	0.04226	0.04350	0.04382
	0.3	2.92E-05	0.00301	0.07364	0.11078	0.11449	0.11542
	0.4	3.97E-05	0.00424	0.14625	0.24049	0.25000	0.25238
	0.5	4.50E-05	0.00496	0.25689	0.48734	0.51115	0.51706
	0.6	4.36E-05	0.00493	0.40776	0.98690	1.05072	1.06622
	0.7	3.54E-05	0.00409	0.56405	2.12498	2.33024	2.37778
	0.8	2.19E-05	0.00258	0.60034	5.26945	6.26407	6.47157
	0.9	7.47E-06	0.00090	0.34884	15.4517	27.9584	30.4737
	0.95	2.17E-06	0.00026	0.13825	19.1087	96.4590	131.180
	0.99	9.73E-08	1.19E-05	0.00879	4.05415	124.402	3466.26
	0.999	1.17E-09	1.23E-07	0.00010	0.09497	7.59731	350836

doi:10.6342/NTU202502609

Table 4 The resistance coefficients for the motion of a soft sphere with $\lambda b = 1$ within an eccentric spherical cavity perpendicular to their common diameter with different values of $d/(c-b)$, b/c, and a/b.

$\frac{d}{(c-b)}$	b/c	$a/b = 0.5$			$a/b = 0.95$		
		F_t	T_r	$-F_r$	F_t	T_r	$-F_r$
0.25	0.1	1.13658	1.00022	0.00063	1.27296	1.00116	0.00372
	0.2	1.31052	1.00164	0.00253	1.70765	1.00887	0.01690
	0.3	1.53410	1.00529	0.00567	2.43650	1.02917	0.04424
	0.4	1.82451	1.01207	0.00990	3.74346	1.06893	0.09470
	0.5	2.20596	1.02288	0.01492	6.30177	1.13822	0.18652
	0.6	2.71281	1.03880	0.02012	11.9425	1.25494	0.36040
	0.7	3.39459	1.06119	0.02437	26.7278	1.45651	0.71955
	0.8	4.32415	1.09197	0.02557	77.9434	1.83817	1.58097
	0.9	5.61329	1.13412	0.01989	382.640	2.73744	4.22017
	0.95	6.44589	1.16086	0.01241	1312.30	3.83630	7.46120
	0.99	7.23124	1.18570	0.00297	5973.18	5.96394	6.92976
	0.999	7.42510	1.19178	0.00031	9588.96	6.89282	1.11704
0.5	0.1	1.14600	1.00049	0.00139	1.29354	1.00262	0.00822
	0.2	1.32730	1.00317	0.00546	1.75361	1.01744	0.03650
	0.3	1.55592	1.00892	0.01196	2.51698	1.05108	0.09399
	0.4	1.84888	1.01804	0.02053	3.87752	1.10976	0.19900
	0.5	2.23024	1.03080	0.03055	6.53011	1.20334	0.38916
	0.6	2.73428	1.04760	0.04081	12.3589	1.35042	0.74799
	0.7	3.41082	1.06934	0.04910	27.5775	1.59019	1.48626
	0.8	4.33373	1.09779	0.05130	80.0005	2.01931	3.24621
	0.9	5.61660	1.13644	0.03981	388.944	2.95805	8.57969
	0.95	6.44690	1.16159	0.02482	1323.17	4.02084	15.0462
	0.99	7.23129	1.18574	0.00593	5977.98	5.99664	13.8706
	0.999	7.42511	1.19178	0.00062	9589.07	6.89335	2.23411

doi:10.6342/NTU202502609

Clearly, $F_t = T_r = 1$ and $F_r = T_t = 0$ (the coupling between particle translation and rotation disappears) as $b/(c-d) = 0$ (the particle is unconfined) for any values of a/b and λb, consistent with equations (1) and (2). Surprisingly and against intuition, as shown in tables 3 and 4, the coupling coefficient F_r (and thus, T_t) is negative for specified values of the parameters a/b, λb, b/c, and $d/(c-b)$. This interesting feature was found and explained in the corresponding translation and rotation of a hard sphere in an eccentric spherical cavity (Lee and Keh 2013a).

3.1 Porous sphere

The force, torque, and coupling coefficients F_t, T_r, and F_r for a porous sphere ($a = 0$) translating and rotating inside an eccentric spherical cavity normal to their common diameter are plotted versus the parameters λb, $d/(c-b)$, and b/c in figures 2-4, respectively. Analogous to the situations of translational and rotational motions of a porous sphere inside a spherical cavity along/about the common diameter (Saad 2016, Chou and Keh 2022, Appendix B), for given values of the parameters λb and $d/(c-b)$, tables 1 and 2 as well as figures 3 and 4 indicate that the normalized force and torque exerted by the fluid on the particle translating and rotating within the cavity normal to their common diameter (or the coefficients F_t and T_r, respectively) increase monotonically with an increase in the particle-to-cavity radius ratio b/c. For fixed

doi:10.6342/NTU202502609

values of λb and b/c, these wall-corrected hydrodynamic force and torque generally increase with increasing relative distance between the particle and cavity centers $d/(c-b)$ (there are exceptions for F_t when b/c is close to unity and λb is finite, as shown in table 1 and figure 3a).

doi:10.6342/NTU202502609

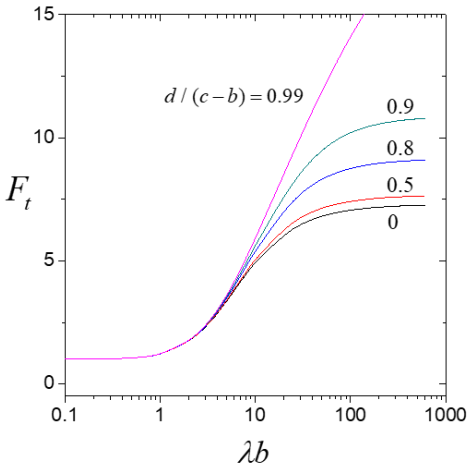

(a)

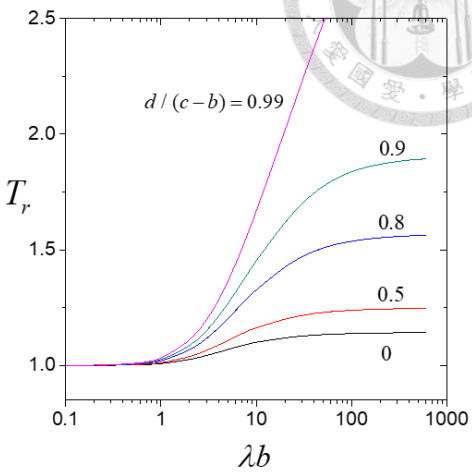

(b)

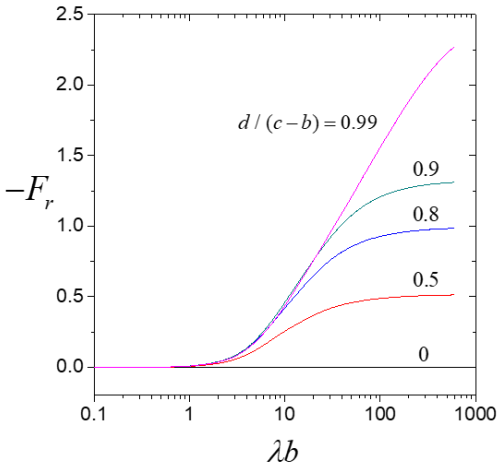

(c)

Figure 2 Resistance coefficients for the translation and rotation of a porous sphere ($a=0$) in an eccentric spherical cavity perpendicular to their common diameter versus the shielding parameter λb with $b/c=1/2$ and $d/(c-b)$ as a parameter: (a) F_t; (b) T_r; (c) F_r.

doi:10.6342/NTU202502609

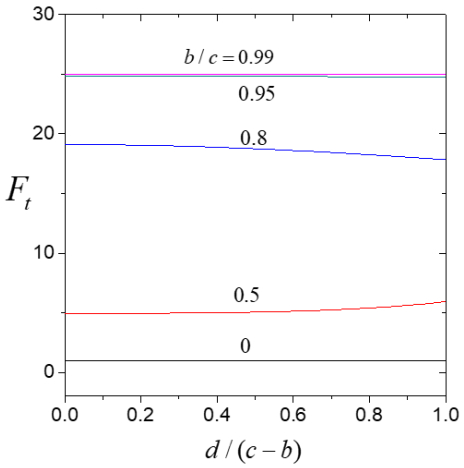

(a)

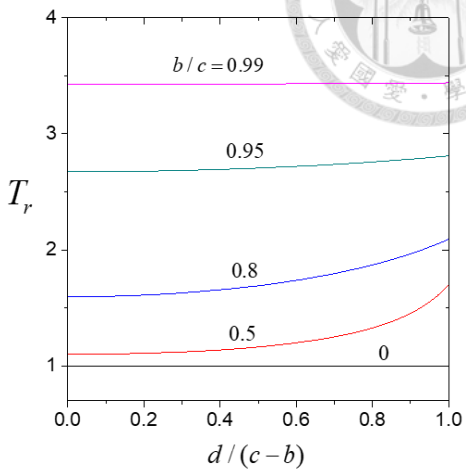

(b)

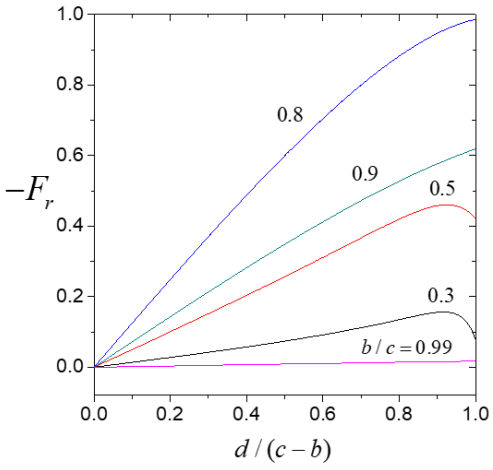

(c)

Figure 3 Resistance coefficients for the translation and rotation of a porous sphere ($a=0$) in an eccentric spherical cavity perpendicular to their common diameter versus the eccentricity parameter $d/(c-b)$ with $\lambda b=10$ and b/c as a parameter: (a) F_t; (b) T_r; (c) F_r.

doi:10.6342/NTU202502609

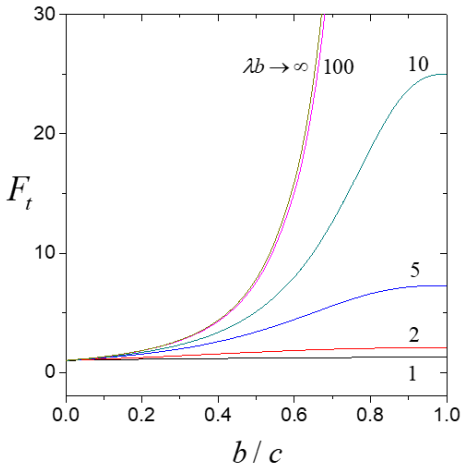

(a)

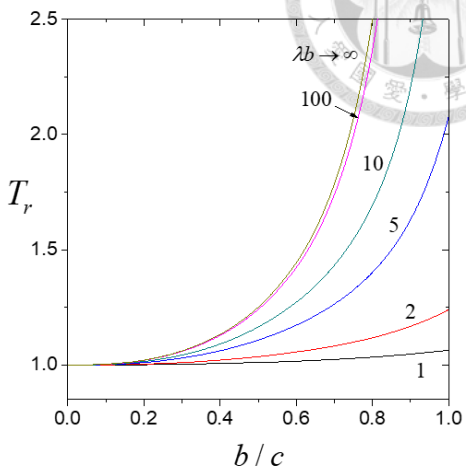

(b)

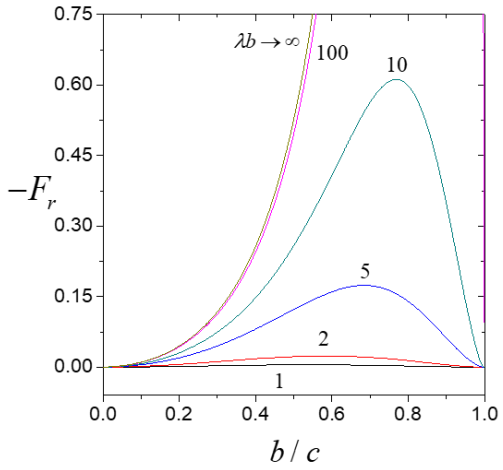

(c)

Figure 4 Resistance coefficients for the translation and rotation of a porous sphere ($a = 0$) in an eccentric spherical cavity perpendicular to their common diameter versus the particle-to-cavity radius ratio b / c with $d / (c - b) = 1 / 2$ and λb as a parameter: (a) F_t; (b) T_r; (c) F_r.

doi:10.6342/NTU202502609

On the other hand, the coupling coefficients F_r and T_t are not necessarily monotonic functions of the parameters b/c and $d/(c-b)$ [there may be maxima in their magnitudes at some moderate values of b/c and $d/(c-b)$], keeping other parameters unchanged. As illustrated in figure 2, all the resistance coefficients F_t, T_r, and F_r increase with an increase in the ratio of particle radius to permeation length λb for constant values of b/c and $d/(c-b)$. Our collocation solutions of F_t and T_r in the concentric limit $d/(c-b)=0$ (given in figures 2 and 3, with $F_r = T_t = 0$ due to the axial symmetry of the translation and rotation) are found to agree excellently with the available analytical solutions (Keh and Chou 2004). A comparison between tables 1 and 2 indicates that the boundary effect of the cavity on the translational motion of the particle is much more pronounced than that on the rotation.

3.2 Composite sphere

The force, torque, and coupling coefficients F_t, T_r, and F_r for a general composite sphere translating and rotating inside an eccentric spherical cavity normal to their common diameter are plotted versus the core-to-particle radius ratio a/b in figures 5 and 6 for various values of the particle-to-cavity radius ratio b/c, shielding parameter λb, and eccentricity parameter $d/(c-b)$. Likewise, F_t and T_r are monotonically

doi:10.6342/NTU202502609

increasing functions of b/c and λb, and generally rise with increasing $d/(c-b)$, keeping other parameters unchanged. The coupling coefficients F_r and T_t increase with an increase in λb, generally increase with an increase in $d/(c-b)$, and are not necessarily monotonic functions of the parameter b/c (there are maxima in their magnitudes at some modest values of b/c, as shown in table 4 and figure 5c). The cavity wall retardation effect on the translation of the composite sphere is much more significant than the effect on the rotation.

doi:10.6342/NTU202502609

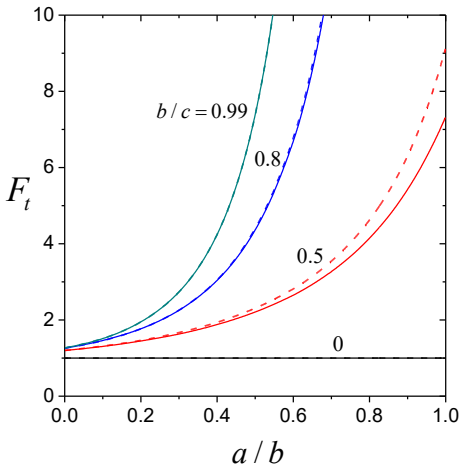

(a)

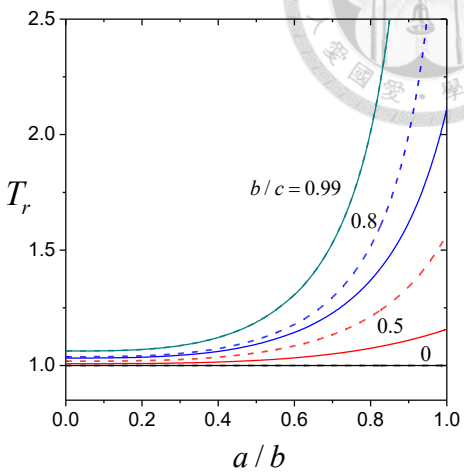

(b)

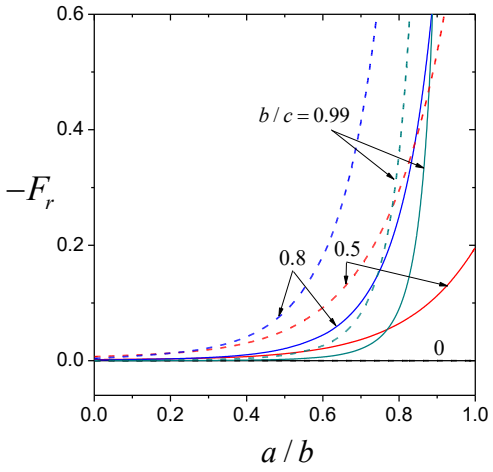

(c)

Figure 5 Resistance coefficients for the translation and rotation of a composite sphere in an eccentric cavity versus the core-to-particle radius ratio a/b with $\lambda b=1$: (a) F_t; (b) T_r; (c) F_r. The dashed and solid curves represent $d/(c-b)=4/5$ and $d/(c-b)=1/5$, respectively.

doi:10.6342/NTU202502609

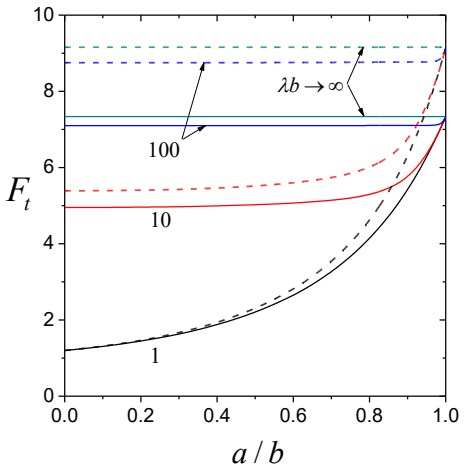

(a)

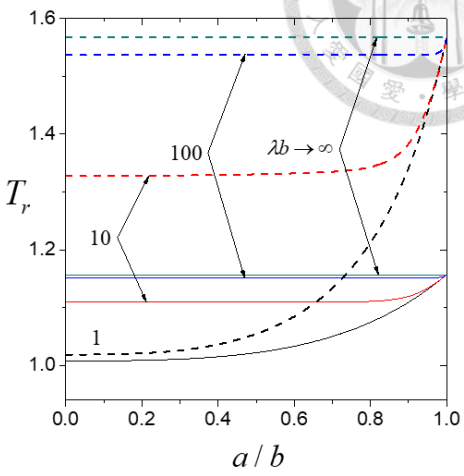

(b)

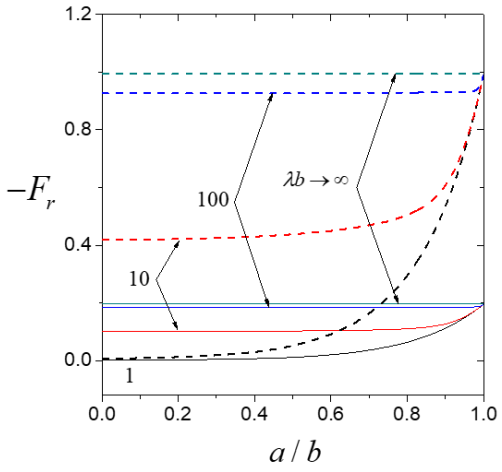

(c)

Figure 6 Resistance coefficients for the translation and rotation of a composite sphere in an eccentric cavity versus the core-to-particle radius ratio a / b with $b / c = 1 / 2$: (a) F_t; (b) T_r; (c) F_r. The dashed and solid curves represent $d / (c - b) = 4 / 5$ and $d / (c - b) = 1 / 5$, respectively.

doi:10.6342/NTU202502609

For given values of b/c, $d/(c-b)$, and λb, figures 5 and 6 and table 4 illustrate that the resistance coefficients F_t and T_r for a translating and rotating composite particle inside an eccentric spherical cavity increase monotonically with increasing core-to-particle radius ratio a/b (become greater if the porous layer is thinner), where cases $a/b=0$ and $a/b=1$ represent entirely porous sphere and hard sphere, respectively. All hydrodynamic force and torque results for a general composite sphere fall between the lower and upper limits of $a/b=0$ and $a/b=1$, respectively. When the surface layer of the composite sphere has slight to modest permeability ($\lambda b \geq 10$), the results of the force, torque, and coupling coefficients for the composite sphere with $a/b \leq 0.8$ inside a spherical cavity can be well approximated by those of an entirely porous sphere within a spherical cavity with the same values of b/c, $d/(c-b)$, and λb, as shown in figure 6. Here, the hard core of the composite particle can hardly feel the relative motion of the fluid and only exerts negligible hydrodynamic resistance. However, this approximation is not suitable for porous layers with high permeability.

Since the governing equations for the general problem of slow translation and rotation of a composite sphere in an arbitrary direction within an eccentric spherical cavity are linear, its solution can be obtained by the superposition of the solutions to its two subproblems: translation and rotation normal to their common diameter, which is investigated in the main text of this thesis, and axisymmetric translation and rotation, as

doi:10.6342/NTU202502609

shown in figure 7. The collocation solutions for the translational/rotational motions of a composite sphere inside an eccentric spherical cavity along/about their common diameter were previously obtained (Chou and Keh 2022, Appendix B). A comparison between these solutions and our results in tables 1, 2, and 4 shows that the cavity wall may exert greater or smaller hydrodynamic force and torque on the particle when its translation/rotation occur along/about the common diameter than the case of translation and rotation perpendicular to it (their differences are generally not significant). Thus, the directions of translation and rotation of a composite sphere inside an eccentric spherical cavity are slightly different from those of the imposed force and torque, respectively, except when they are oriented along/about or normal to the common diameter.

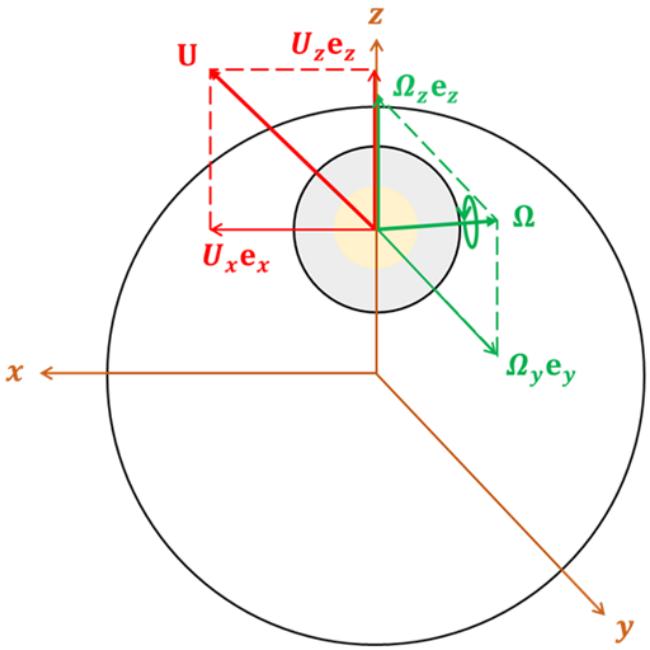

Figure 7 Geometrical sketch of the translation and rotation of a composite sphere in arbitrary directions within an eccentric spherical cavity.

doi:10.6342/NTU202502609

The physical meanings for the four dimensionless parameters a/b, b/c, $d/(c-b)$, and λb are graphically depicted in figure 8.

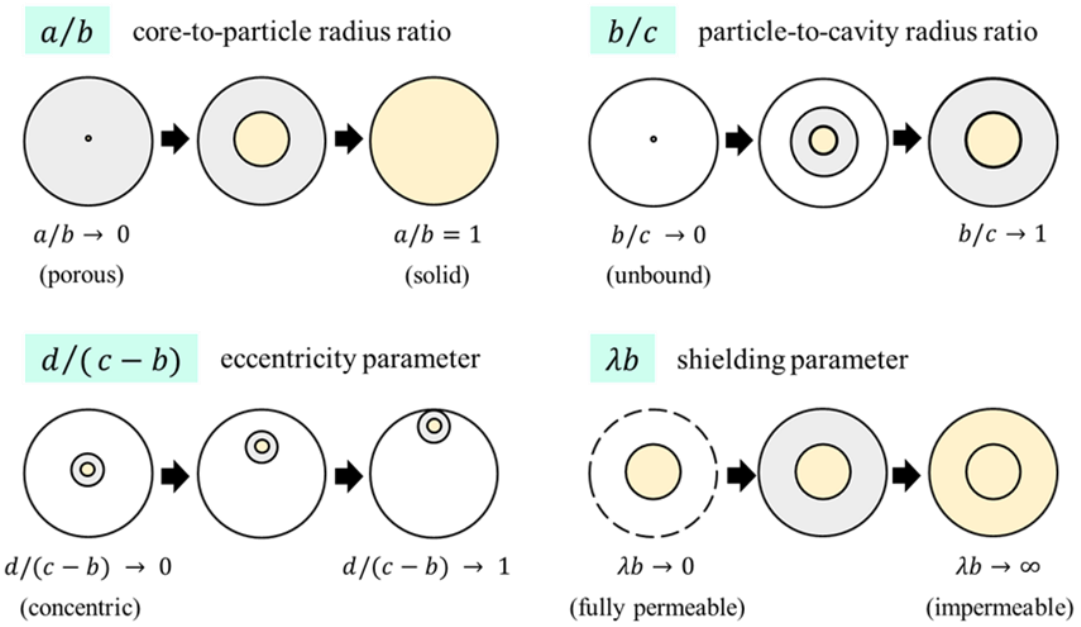

Figure 8 Schematic diagram of the physical meanings for the dimensionless parameters a/b, b/c, $d/(c-b)$, and λb.

doi:10.6342/NTU202502609

Chapter 4

Conclusions

In the main text of this thesis, the slow coupled translation and rotation of a composite sphere, which is a hard sphere core coated with a permeable porous layer, in an incompressible Newtonian fluid inside an eccentric spherical cavity normal to their common diameter in the quasi-steady state is semi-analytically studied by using a boundary collocation method. Accurate solutions of the force and torque exerted by the fluid on the composite sphere are obtained for wide-range values of the ratio of particle radius to porous layer permeation length λb, particle-to-cavity radius ratio b/c, core-to-particle radius ratio a/b, and relative distance between the particle and cavity centers $d/(c-b)$. The force and torque on a translating and rotating particle increase monotonically with an increase in λb, a/b, or b/c, and generally increase with increasing $d/(c-b)$. The boundary effect of the cavity on the translation of the particle is much more pronounced than that on the rotation. The coupling effect in the simultaneous translation and rotation inside an eccentric spherical cavity is complicated and not a monotonic function of b/c.

In tables 1-4 and figures 2-6, we give results for the resistance problem, defined as

doi:10.6342/NTU202502609

the problem of determining the hydrodynamic force $\mathbf{F}$ and torque $\mathbf{T}$ on a composite sphere for specified quasi-steady particle velocities $\mathbf{U}$ and $\mathbf{\Omega}$ within an eccentric spherical cavity. In the mobility problem, the external force $\mathbf{F}$ and torque $\mathbf{T}$ acting on the composite sphere have been given, and the particle velocities $\mathbf{U}$ and $\mathbf{\Omega}$ need to be determined. For the slow translation and rotation of a composite sphere within an eccentric spherical cavity perpendicular to their common diameter considered here, our expressions in equations (20) and (21) may also be applied to its matching mobility problem where the external force and torque on the composite sphere are given and thus the composite sphere translates and rotates accordingly. For example, the translational and angular velocities of a composite sphere under the condition of free rotation within an eccentric spherical cavity normal to their common diameter driven by the external force $F\mathbf{e}_x$ can be obtained using equations (20) and (21), with the result

$$U = \frac{F}{F_0 / U}\left(F_t - F_r \frac{T_t}{T_r}\right)^{-1}, \tag{23a}$$

$$\Omega = -\frac{U}{b}\frac{T_t}{T_r}, \tag{23b}$$

where the resistance coefficients in equation (23) have been given in the tables and figures in the previous chapters and the value of F_0 / U on the right-hand side of equation (23a) can be calculated using equation (1).

doi:10.6342/NTU202502609

List of Symbols

a	the radius of the hard core of the composite sphere, [m]
A_{in}, B_{in}, C_{in}	unknown constants in Eqs. (11) and (12)
$\hat{A}_{in}, \hat{B}_{in}, \hat{C}_{in}$	unknown constants in Eq. (14)
$A_{in}^{*}, B_{in}^{*}, C_{in}^{*}$	position functions given by Eqs. (A13)-(A17)
$A_{in}^{**}, B_{in}^{**}, C_{in}^{**}$	position functions given by Eqs. (A22)-(A27)
$A_{in}^{***}, B_{in}^{***}, C_{in}^{***}$	position functions given by Eqs. (A34)-(A39)
$A_{in}^{'}, C_{in}^{'}$	position functions given by Eqs. (A18)-(A21)
$A_{in}^{''}, B_{in}^{''}, C_{in}^{''}$	position functions given by Eqs. (A28)-(A33)
$A_{in}^{'''}, B_{in}^{'''}, C_{in}^{'''}$	position functions given by Eqs. (A40)-(A45)
b	the radius of the composite sphere, [m]
c	the radius of the cavity, [m]
d	the distance between the cavity center and the particle center, [m]
$\mathbf{e}_{ri}, \mathbf{e}_{\theta i}, \mathbf{e}_{\phi}$	principal unit vectors in the ith spherical coordinate system

doi:10.6342/NTU202502609

$\mathbf{e}_x, \mathbf{e}_y, \mathbf{e}_z$	principal unit vectors in Cartesian coordinates
$f^{(1)}, f^{(2)}$	the functions used for coordinate transformation
$\mathbf{F}, F$	the drag force exerted on the composite sphere by the fluid, [N]
$\mathbf{F_0}, F_0$	the drag force exerted on a composite sphere by an unbounded fluid, [N]
F_t, F_r, T_t, T_r	the dimensionless resistance coefficients
$\mathbf{I}$	unit dyadic
I_n	the modified Bessel function of the first kind of order n
K_n	the modified Bessel function of the second kind of order n
p	dynamic pressure for the external fluid, [Pa]
p_1	the component of p generated by the particle, [Pa]
p_2	the component of p generated by the cavity, [Pa]
$\hat{p}$	dynamic pressure for the internal fluid, [Pa]
P_n^1	the associated Legendre function of the first kind of order n and degree 1

doi:10.6342/NTU202502609

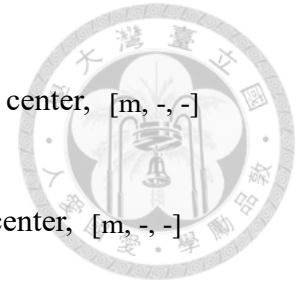

r_1, θ_1, ϕ	spherical coordinates originated from the particle center, [m, -, -]
r_2, θ_2, ϕ	spherical coordinates originated from the cavity center, [m, -, -]
$\mathbf{T}, T$	the torque exerted on the composite sphere by the fluid, $[\mathrm{N \cdot m}]$
$\mathbf{T_0}, T_0$	the torque exerted on a composite sphere by an unbounded fluid, $[\mathrm{N \cdot m}]$
$\mathbf{U}, U$	the translational velocity of the composite sphere, $[\mathrm{m \cdot s^{-1}}]$
$\mathbf{v}$	velocity field for the external fluid, $[\mathrm{m \cdot s^{-1}}]$
$\mathbf{v}_1$	the component of $\mathbf{v}$ generated by the particle, $[\mathrm{m \cdot s^{-1}}]$
$\mathbf{v}_2$	the component of $\mathbf{v}$ generated by the cavity, $[\mathrm{m \cdot s^{-1}}]$
$\hat{\mathbf{v}}$	velocity field for the internal fluid, $[\mathrm{m \cdot s^{-1}}]$
$v_{ir}, v_{i\theta}, v_{i\phi}$	components of $\mathbf{v}_i$ in spherical coordinates, $[\mathrm{m \cdot s^{-1}}]$
$\hat{v}_r, \hat{v}_\theta, \hat{v}_\phi$	components of $\hat{\mathbf{v}}$ in spherical coordinates, $[\mathrm{m \cdot s^{-1}}]$
x, y, z	Cartesian coordinates originated from the cavity center, [m, m, m]

doi:10.6342/NTU202502609

Greek letters

$\Gamma_1^{(k)} \sim \Gamma_5^{(k)}$	position functions given by Eqs. (A46)-(A50)
η	the viscosity of the fluid, $[\mathrm{kg \cdot m^{-1} \cdot s^{-1}}]$
λ	the reciprocal of the square root of the fluid permeability or flow penetration length in the porous layer, $[\mathrm{m^{-1}}]$
μ_i	$= \cos\theta_i$
ρ, ϕ, z	cylindrical coordinates originated from the cavity center, [m, -, m]
$\boldsymbol{\tau}$	the viscous stress tensor of the external fluid, $[\mathrm{N \cdot m^{-2}}]$
$\hat{\boldsymbol{\tau}}$	the viscous stress tensor of the internal fluid, $[\mathrm{N \cdot m^{-2}}]$
$\boldsymbol{\Omega}, \Omega$	the angular velocity of the composite sphere, $[\mathrm{s^{-1}}]$

doi:10.6342/NTU202502609

References

Anderson J L 1989 Colloid transport by interfacial forces *Ann. Rev. Fluid Mech.* **21** 61–99

Anderson J L and Solomentsev Y 1996 Hydrodynamic effects of surface layer on colloidal particles *Chem. Eng. Commun.* **148–150** 291–314

Brenner H 1961 The slow motion of a sphere through a viscous fluid towards a plane surface *Chem. Eng. Sci.* **16** 242–251

Brenner H and Sonshine R M 1964 Slow viscous rotation of a sphere in a circular cylinder *Quart. J. Mech. Appl. Math.* **17** 55-63

Bungay P M and Brenner H 1973 The motion of a closely-fitting sphere in a fluid-filled tube *Int. J. Multiph. Flow* **1** 25–56

Chang C L and Keh H J 2023 Slow rotation of a soft colloidal sphere normal to two plane walls *Colloids Interfaces* **7** 18

Chang Y C and Keh H J 2006 Slow motion of a slip spherical particle perpendicular to two plane walls *J. Fluids Struct.* **22** 647–661

Chen P Y and Keh H J 2003 Slow motion of a slip spherical particle parallel to one or two plane walls *J. Chin. Inst. Chem. Eng.* **34** 123–133

Chen S B 1998 Axisymmetric motion of multiple composite spheres: Solid core with permeable shell, under creeping flow conditions *Phys. Fluids* **10** 1550–1563

Chen S B and Ye X 2000 Boundary effect on slow motion of a composite sphere perpendicular to two parallel impermeable plates *Chem. Eng. Sci.* **55** 2441–2453

Chou C Y and Keh H J 2021 Slow rotation of a spherical particle in an eccentric spherical cavity with slip surfaces *Eur. J. Mech.* B **86** 150-156

doi:10.6342/NTU202502609

Chou C Y and Keh H J 2022 Low-Reynolds-number rotation of a soft particle inside an eccentric cavity *Eur. J. Mech.* B **91** 194–201

Dean W R and O'Neill M E 1963 A slow motion of viscous liquid caused by the rotation of a solid sphere *Mathematika* **10** 13-24

Ganatos P, Weinbaum S and Pfeffer R 1980a A strong interaction theory for the creeping motion of a sphere between plane parallel boundaries Part 1 Perpendicular motion *J. Fluid Mech.* **99** 739-753

Ganatos P, Weinbaum S and Pfeffer R 1980b A strong interaction theory for the creeping motion of a sphere between plane parallel boundaries Part 2 Parallel motion *J. Fluid Mech.* **99** 755-783

Goldman A J, Cox R G and Brenner H 1967 Slow viscous motion of a sphere parallel to a plane wall - I. Motion through a quiescent fluid *Chem. Eng. Sci.* **22** 637–651

Greenstein T and Schiavina G L 1975 Torque exerted on a slowly rotating eccentrically positioned sphere within an infinitely long circular cylinder *Int. J. Multiphase Flow* **2** 353-355

Happel J and Brenner H 1983 *Low Reynolds Number Hydrodynamics* (Dordrecht, Netherlands: Nijhoff)

Jhuang L J and Keh H J 2022 Slow axisymmetric rotation of a soft sphere in a circular cylinder *Eur. J. Mech. B Fluids* **95** 205–211

Keh H J and Chang J H 1998 Boundary effects on the creeping-flow and thermophoretic motions of an aerosol particle in a spherical cavity *Chem. Eng. Sci.* **53** 2365–2377

Keh H J and Chang Y C 2007 Creeping motion of a slip spherical particle in a circular cylindrical pore *Int. J. Multiph. Flow* **33** 726–741

Keh H J and Chou J 2004 Creeping motion of a composite sphere in a concentric spherical

doi:10.6342/NTU202502609

cavity *Chem. Eng. Sci.* **59** 407–415

Keh H J and Lee T C 2010 Axisymmetric creeping motion of a slip spherical particle in a nonconcentric spherical cavity *Theor. Comput. Fluid Dyn.* **24** 497–510

Koplik J, Levine H and Zee A 1983 Viscosity renormalization in the Brinkman equation *Phys. Fluids* **26** 2864–2870

Krishna Prasad M 2021 Boundary effects of a nonconcentric semipermeable sphere using Happel and Kuwabara cell models *Appl. Comput. Mech.* **15** 19–30

Lee M C and Keh H J 2021 Slow axisymmetric rotation of a sphere in a circular tube with slip surfaces *Fluid Dyn. Res.* **53** 065502

Lee T C and Keh H J 2013a Slow motion of a spherical particle in a spherical cavity with slip surfaces *Int. J. Eng. Sci.* **69** 1-15

Lee T C and Keh H J 2013b Axisymmetric thermocapillary migration of a fluid sphere in a spherical cavity *Int. J. Heat Mass Transfer* **62** 772-781

Leichtberg S, Pfeffer R and Weinbaum S 1976 Stokes flow past finite coaxial clusters of spheres in a circular cylinder *Int. J. Multiph. Flow* **3** 147–169

Liao J C and Keh H J 2022 Slow rotation of a sphere about its diameter normal to two planes with slip surfaces *Fluid Dyn. Res.* **54** 035502

Malysa K and van de Ven T G M 1986 Rotational and translational motion of a sphere parallel to a wall *Int. J. Multiph. Flow* **12** 459–468

Masliyah J H, Neale G, Malysa K and van de Ven T G M 1987 Creeping flow over a composite sphere: Solid core with porous shell *Chem. Eng. Sci.* **42** 245–253

Napper D H 1983 *Polymeric Stabilization of Colloidal Dispersions* (London: Academic Press)

Neale G, Epstein N and Nader W 1973 Creeping flow relative to permeable spheres *Chem.*

doi:10.6342/NTU202502609

Eng. Sci. **28** 1865-1874

Papavassiliou D and Alexander G P 2017 Exact solutions for hydrodynamic interactions of two squirming spheres *J. Fluid Mech.* **813** 618-646

Prakash J and Raja Sekhar G P 2017 Slow motion of a porous spherical particle with a rigid core in a spherical fluid cavity *Meccanica* **52** 91–105

Romanò F, des Boscs P-E and Kuhlmann H C 2020 Forces and torques on a sphere moving near a dihedral corner in creeping flow *Eur. J. Mech.* B **84** 110-121

Saad E I 2016 Axisymmetric motion of a porous sphere through a spherical envelope subject to a stress jump condition *Meccanica* **51** 799–817

Sherief H H, Faltas M S and Saad E I 2016 Stokes resistance of a porous spherical particle in a spherical cavity *Acta Mech.* **227** 1075–1093

Srinivasacharya D and Krishna Prasad M 2012 Steady rotation of a composite sphere in a concentric spherical cavity *Acta Mech. Sin.* **28** 653–658

Stokes G G 1845 On the theories of the internal friction of fluids in motion and of the equilibrium and motion of elastic solids *Trans. Camb. Phil. Soc.* **8** 287-319

Stokes G G 1851 On the effect of the internal friction of fluids on the motion of pendulums *Trans. Camb. Phil. Soc.* **9** 8-106

Wunderlich R W 1982 The effects of surface structure on the electrophoretic mobilities of large particles *J. Colloid Interface Sci.* **88** 385–397

doi:10.6342/NTU202502609

Appendix A

Equations to Be Solved for Unknown Constants in Equations (9)-(14)

Applying the boundary conditions given by equations (6)-(8) to equations (9)-(14), we obtain

$$\sum_{n=1}^{\infty} n(n+1)\{\hat{C}_{2n}a^{n-1}+\hat{C}_{1n}a^{-n-2}$$

$$+\lambda^{-1/2}a^{-3/2}[\hat{A}_{2n}I_{n+1/2}(\lambda a)+\hat{A}_{1n}K_{n+1/2}(\lambda a)]\}P_n^1(\mu_1)=0\,, \tag{A1}$$

$$\sum_{n=1}^{\infty}\{(\lambda a)^{-1/2}[\hat{B}_{2n}I_{n+1/2}(\lambda a)+\hat{B}_{1n}K_{n+1/2}(\lambda a)]P_n^1(\mu_1)(1-\mu_1^{\,2})^{-1/2}$$

$$+[\hat{C}_{2n}(-n-1)a^{n-1}+\hat{C}_{1n}na^{-n-2}+\lambda^{-1/2}a^{-3/2}\{\hat{A}_{2n}[nI_{n+1/2}(\lambda a)-\lambda aI_{n-1/2}(\lambda a)]$$

$$+\hat{A}_{1n}[nK_{n+1/2}(\lambda a)+\lambda aK_{n-1/2}(\lambda a)]\}]\frac{\mathrm{d}P_n^1(\mu_1)}{\mathrm{d}\mu_1}(1-\mu_1^{\,2})^{1/2}\}=0\,, \tag{A2}$$

$$\sum_{n=1}^{\infty}\{(\lambda a)^{-1/2}[\hat{B}_{2n}I_{n+1/2}(\lambda a)+\hat{B}_{1n}K_{n+1/2}(\lambda a)]\frac{\mathrm{d}P_n^1(\mu_1)}{\mathrm{d}\mu_1}(1-\mu_1^{\,2})^{1/2}$$

$$+[\hat{C}_{2n}(-n-1)a^{n-1}+\hat{C}_{1n}na^{-n-2}+\lambda^{-1/2}a^{-3/2}\{\hat{A}_{2n}[nI_{n+1/2}(\lambda a)-\lambda aI_{n-1/2}(\lambda a)]$$

$$+\hat{A}_{1n}[nK_{n+1/2}(\lambda a)+\lambda aK_{n-1/2}(\lambda a)]\}]P_n^1(\mu_1)(1-\mu_1^{\,2})^{-1/2}\}=0\,; \tag{A3}$$

$$\sum_{n=1}^{\infty}\{[(n+1)(C_{1n}b^{-n-2}+A_{1n}b^{-n})$$

$$-n(n+1)\{\hat{C}_{2n}b^{n-1}+\hat{C}_{1n}b^{-n-2}+\lambda^{-1/2}b^{-3/2}[\hat{A}_{2n}I_{n+1/2}(\lambda b)+\hat{A}_{1n}K_{n+1/2}(\lambda b)]\}]P_n^1(\mu_1)$$

$$+[C_{2n}\{nf^{(1)}P_n^1(\mu_2)+f^{(2)}\frac{\mathrm{d}P_n^1(\mu_2)}{\mathrm{d}\mu_2}(1-\mu_2^{\,2})^{1/2}\}r_2^{\,n-1}-B_{2n}f^{(2)}r_2^{\,n}P_n^1(\mu_2)(1-\mu_2^{\,2})^{-1/2}$$

doi:10.6342/NTU202502609

$$+A_{2n}\{nf^{(1)}P_n^1(\mu_2)+\frac{n+3}{n+1}f^{(2)}\frac{\mathrm{d}P_n^1(\mu_2)}{\mathrm{d}\mu_2}(1-\mu_2{}^2)^{1/2}\}r_2{}^{n+1}]_{r_1=b}\}=U(1-\mu_1{}^2)^{1/2}, \quad \text{(A4)}$$

$$\sum_{n=1}^{\infty}\{[B_{1n}b^{-n-1}-(\lambda b)^{-1/2}\{\hat{B}_{2n}I_{n+1/2}(\lambda b)+\hat{B}_{1n}K_{n+1/2}(\lambda b)\}]P_n^1(\mu_1)(1-\mu_1{}^2)^{-1/2}$$

$$+[C_{1n}b^{-n-2}+A_{1n}\frac{n-2}{n}b^{-n}-\hat{C}_{2n}(-n-1)b^{n-1}-\hat{C}_{1n}nb^{-n-2}-\lambda^{-1/2}b^{-3/2}\{\hat{A}_{2n}[nI_{n+1/2}(\lambda b)$$

$$-\lambda bI_{n-1/2}(\lambda b)]+\hat{A}_{1n}[nK_{n+1/2}(\lambda b)+\lambda bK_{n-1/2}(\lambda b)]\}]\frac{\mathrm{d}P_n^1(\mu_1)}{\mathrm{d}\mu_1}(1-\mu_1{}^2)^{1/2}$$

$$+[B_{2n}f^{(1)}r_2{}^nP_n^1(\mu_2)(1-\mu_2{}^2)^{-1/2}+C_{2n}\{nf^{(2)}P_n^1(\mu_2)-f^{(1)}\frac{\mathrm{d}P_n^1(\mu_2)}{\mathrm{d}\mu_2}(1-\mu_2{}^2)^{1/2}\}r_2{}^{n-1}$$

$$+A_{2n}\{nf^{(2)}P_n^1(\mu_2)-\frac{n+3}{n+1}f^{(1)}\frac{\mathrm{d}P_n^1(\mu_2)}{\mathrm{d}\mu_2}(1-\mu_2{}^2)^{1/2}\}r_2{}^{n+1}]_{r_1=b}\}=U\mu_1+b\Omega, \quad \text{(A5)}$$

$$\sum_{n=1}^{\infty}\{[B_{1n}b^{-n-1}-(\lambda b)^{-1/2}\{\hat{B}_{2n}I_{n+1/2}(\lambda b)+\hat{B}_{1n}K_{n+1/2}(\lambda b)\}]\frac{\mathrm{d}P_n^1(\mu_1)}{\mathrm{d}\mu_1}(1-\mu_1{}^2)^{1/2}+[C_{1n}b^{-n-2}$$

$$+A_{1n}\frac{n-2}{n}b^{-n}-\hat{C}_{2n}(-n-1)b^{n-1}-\hat{C}_{1n}nb^{-n-2}-\lambda^{-1/2}b^{-3/2}\{\hat{A}_{2n}[nI_{n+1/2}(\lambda b)-\lambda bI_{n-1/2}(\lambda b)]$$

$$+\hat{A}_{1n}[nK_{n+1/2}(\lambda b)+\lambda bK_{n-1/2}(\lambda b)]\}]P_n^1(\mu_1)(1-\mu_1{}^2)^{-1/2}+[B_{2n}r_2{}^n\frac{\mathrm{d}P_n^1(\mu_2)}{\mathrm{d}\mu_2}(1-\mu_2{}^2)^{1/2}$$

$$-(C_{2n}r_2{}^{n-1}+A_{2n}\frac{n+3}{n+1}r_2{}^{n+1})P_n^1(\mu_2)(1-\mu_2{}^2)^{-1/2}]_{r_1=b}\}=-U-b\Omega\mu_1, \quad \text{(A6)}$$

$$\sum_{n=1}^{\infty}[(C_{1n}C_{1n}^*+A_{1n}A_{1n}^*+B_{2n}B_{2n}^*+C_{2n}C_{2n}^*+A_{2n}A_{2n}^*)$$

$$-(\hat{C}_{2n}C_{2n}^{'}+\hat{C}_{1n}C_{1n}^{'}+\hat{A}_{2n}A_{2n}^{'}+\hat{A}_{1n}A_{1n}^{'})]_{r_1=b}=0, \quad \text{(A7)}$$

$$\sum_{n=1}^{\infty}[(B_{1n}B_{1n}^{**}+C_{1n}C_{1n}^{**}+A_{1n}A_{1n}^{**}+B_{2n}B_{2n}^{**}+C_{2n}C_{2n}^{**}+A_{2n}A_{2n}^{**})$$

$$-(\hat{B}_{2n}B_{2n}^{''}+\hat{B}_{1n}B_{1n}^{''}+\hat{C}_{2n}C_{2n}^{''}+\hat{C}_{1n}C_{1n}^{''}+\hat{A}_{2n}A_{2n}^{''}+\hat{A}_{1n}A_{1n}^{''})]_{r_1=b}=0, \quad \text{(A8)}$$

doi:10.6342/NTU202502609

$$\sum_{n=1}^{\infty}[(B_{1n}B_{1n}^{***}+C_{1n}C_{1n}^{***}+A_{1n}A_{1n}^{***}+B_{2n}B_{2n}^{***}+C_{2n}C_{2n}^{***}+A_{2n}A_{2n}^{***})$$

$$-(\hat{B}_{2n}B_{2n}^{'''}+\hat{B}_{1n}B_{1n}^{'''}+\hat{C}_{2n}C_{2n}^{'''}+\hat{C}_{1n}C_{1n}^{'''}+\hat{A}_{2n}A_{2n}^{'''}+\hat{A}_{1n}A_{1n}^{'''})]_{r_1=b}=0; \quad \text{(A9)}$$

$$\sum_{n=1}^{\infty}\{[B_{1n}f^{(2)}r_1^{-n-1}P_n^1(\mu_1)(1-\mu_1^2)^{-1/2}$$

$$+C_{1n}\{(n+1)f^{(1)}P_n^1(\mu_1)+f^{(2)}\frac{\mathrm{d}P_n^1(\mu_1)}{\mathrm{d}\mu_1}(1-\mu_1^2)^{1/2}\}r_1^{-n-2}$$

$$+A_{1n}\{(n+1)f^{(1)}P_n^1(\mu_1)+\frac{n-2}{n}f^{(2)}\frac{\mathrm{d}P_n^1(\mu_1)}{\mathrm{d}\mu_1}(1-\mu_1^2)^{1/2}\}r_1^{-n}]_{r_2=c}$$

$$+nP_n^1(\mu_2)(C_{2n}c^{n-1}+A_{2n}c^{n+1})\}=0, \quad \text{(A10)}$$

$$\sum_{n=1}^{\infty}\{[B_{1n}f^{(1)}r_1^{-n-1}P_n^1(\mu_1)(1-\mu_1^2)^{-1/2}$$

$$-C_{1n}\{(n+1)f^{(2)}P_n^1(\mu_1)-f^{(1)}\frac{\mathrm{d}P_n^1(\mu_1)}{\mathrm{d}\mu_1}(1-\mu_1^2)^{1/2}\}r_1^{-n-2}$$

$$-A_{1n}\{(n+1)f^{(2)}P_n^1(\mu_1)-\frac{n-2}{n}f^{(1)}\frac{\mathrm{d}P_n^1(\mu_1)}{\mathrm{d}\mu_1}(1-\mu_1^2)^{1/2}\}r_1^{-n}]_{r_2=c}$$

$$+B_{2n}c^nP_n^1(\mu_2)(1-\mu_2^2)^{-1/2}-(C_{2n}c^{n-1}+A_{2n}\frac{n+3}{n+1}c^{n+1})\frac{\mathrm{d}P_n^1(\mu_2)}{\mathrm{d}\mu_2}(1-\mu_2^2)^{1/2}\}=0, \quad \text{(A11)}$$

$$\sum_{n=1}^{\infty}\{[B_{1n}r_1^{-n-1}\frac{\mathrm{d}P_n^1(\mu_1)}{\mathrm{d}\mu_1}(1-\mu_1^2)^{1/2}+(C_{1n}r_1^{-n-2}+A_{1n}\frac{n-2}{n}r_1^{-n})P_n^1(\mu_1)(1-\mu_1^2)^{-1/2}]_{r_2=c}$$

$$+B_{2n}c^n\frac{\mathrm{d}P_n^1(\mu_2)}{\mathrm{d}\mu_2}(1-\mu_2^2)^{1/2}-(C_{2n}c^{n-1}+A_{2n}\frac{n+3}{n+1}c^{n+1})P_n^1(\mu_2)(1-\mu_2^2)^{-1/2}\}=0. \quad \text{(A12)}$$

Here, A_{in}, B_{in}, and C_{in} with asterisks and apostrophes for $i=1$ and 2 in equations (A7)-(A9) are the position functions given by

doi:10.6342/NTU202502609

$$A_{1n}^{*} = -2(n^2+3n-1)r_1^{-n-1}P_n^1(\mu_1), \tag{A13}$$

$$C_{1n}^{*} = -2(n+1)(n+2)r_1^{-n-3}P_n^1(\mu_1), \tag{A14}$$

$$A_{2n}^{*} = 2r_2^{n+1}\{[n\frac{\partial f^{(1)}}{\partial r_1} + r_2^{-1}\{n(n+1)\frac{\partial r_2}{\partial r_1}f^{(1)} - (2n+3)\}]P_n^1(\mu_2)$$

$$+[\frac{n+3}{n+1}\frac{\partial f^{(2)}}{\partial r_1} + (n+3)r_2^{-1}\frac{\partial r_2}{\partial r_1}f^{(2)} - n\frac{\partial \theta_2}{\partial r_1}f^{(1)}]\frac{\mathrm{d}P_n^1(\mu_2)}{\mathrm{d}\mu_2}(1-\mu_2^{\,2})^{1/2}$$

$$+\frac{n+3}{n+1}\frac{\partial \theta_2}{\partial r_1}f^{(2)}[\frac{\mathrm{d}P_n^1(\mu_2)}{\mathrm{d}\mu_2}\mu_2 - \frac{\mathrm{d}^2P_n^1(\mu_2)}{\mathrm{d}\mu_2^{\,2}}(1-\mu_2^{\,2})]\}, \tag{A15}$$

$$B_{2n}^{*} = 2r_2^{n}\{[-\frac{\partial f^{(2)}}{\partial r_1} - nr_2^{-1}\frac{\partial r_2}{\partial r_1}f^{(2)}]P_n^1(\mu_2)(1-\mu_2^{\,2})^{-1/2}$$

$$+\frac{\partial \theta_2}{\partial r_1}f^{(2)}[\frac{\mathrm{d}P_n^1(\mu_2)}{\mathrm{d}\mu_2} + P_n^1(\mu_2)\mu_2(1-\mu_2^{\,2})^{-1}]\}, \tag{A16}$$

$$C_{2n}^{*} = 2r_2^{n-1}\{[n\frac{\partial f^{(1)}}{\partial r_1} + n(n-1)r_2^{-1}\frac{\partial r_2}{\partial r_1}f^{(1)}]P_n^1(\mu_2)$$

$$+[\frac{\partial f^{(2)}}{\partial r_1} + (n-1)r_2^{-1}\frac{\partial r_2}{\partial r_1}f^{(2)} - n\frac{\partial \theta_2}{\partial r_1}f^{(1)}]\frac{\mathrm{d}P_n^1(\mu_2)}{\mathrm{d}\mu_2}(1-\mu_2^{\,2})^{1/2}$$

$$+\frac{\partial \theta_2}{\partial r_1}f^{(2)}[\frac{\mathrm{d}P_n^1(\mu_2)}{\mathrm{d}\mu_2}\mu_2 - \frac{\mathrm{d}^2P_n^1(\mu_2)}{\mathrm{d}\mu_2^{\,2}}(1-\mu_2^{\,2})]\}, \tag{A17}$$

$$A_{1n}^{'} = 2n(n+1)\lambda^{-1/2}r_1^{-5/2}(-\lambda r_1 K_{n-1/2}(\lambda r_1) - (n+2)K_{n+1/2}(\lambda r_1))P_n^1(\mu_1), \tag{A18}$$

$$C_{1n}^{'} = -n(2n^2+6n+4+\lambda^2 r_1^2)r_1^{-n-3}P_n^1(\mu_1), \tag{A19}$$

$$A_{2n}^{'} = 2n(n+1)\lambda^{-1/2}r_1^{-5/2}(\lambda r_1 I_{n-1/2}(\lambda r_1) - (n+2)I_{n+1/2}(\lambda r_1))P_n^1(\mu_1), \tag{A20}$$

$$C_{2n}^{'} = (n+1)(2n^2-2n+\lambda^2 r_1^2)r_1^{n-2}P_n^1(\mu_1), \tag{A21}$$

$$A_{1n}^{**} = -2\frac{(n+1)(n-1)}{n}r_1^{-n-1}\frac{\mathrm{d}P_n^1(\mu_1)}{\mathrm{d}\mu_1}(1-\mu_1^{\,2})^{1/2}, \tag{A22}$$

doi:10.6342/NTU202502609

$$B_{1n}^{**} = -(n+2)r_1^{-n-2}P_n^1(\mu_1)(1-\mu_1^2)^{-1/2}, \tag{A23}$$

$$C_{1n}^{**} = -2(n+2)r_1^{-n-3}\frac{\mathrm{d}P_n^1(\mu_1)}{\mathrm{d}\mu_1}(1-\mu_1^2)^{1/2}, \tag{A24}$$

$$A_{2n}^{**} = r_2^{n+1}[\Gamma_1^{(2)} + \Gamma_2^{(2)} + \Gamma_3^{(2)}], \tag{A25}$$

$$\begin{aligned} B_{2n}^{**} = r_2^{n}\{&[nr_2^{-1}\frac{\partial r_2}{\partial r_1}f^{(1)} + \frac{\partial f^{(1)}}{\partial r_1} \\ &-r_1^{-1}(nr_2^{-1}\frac{\partial r_2}{\partial \theta_1}f^{(2)} + f^{(1)} + \frac{\partial f^{(2)}}{\partial \theta_1})]P_n^1(\mu_2)(1-\mu_2^2)^{-1/2} \\ &+[r_1^{-1}\frac{\partial \theta_2}{\partial \theta_1}f^{(2)} - \frac{\partial \theta_2}{\partial r_1}f^{(1)}][\frac{\mathrm{d}P_n^1(\mu_2)}{\mathrm{d}\mu_2} + P_n^1(\mu_2)\mu_2(1-\mu_2^2)^{-1}]\}, \end{aligned} \tag{A26}$$

$$C_{2n}^{**} = r_2^{n-1}[\Gamma_1^{(1)} + \Gamma_2^{(1)} + \Gamma_3^{(1)}], \tag{A27}$$

$$\begin{aligned} A_{1n}^{"} = \lambda^{-1/2}r_1^{-5/2}(&-(2n^2+4n+\lambda^2r_1^2)K_{n+1/2}(\lambda r_1) \\ &-2\lambda r_1 K_{n-1/2}(\lambda r_1))\frac{\mathrm{d}P_n^1(\mu_1)}{\mathrm{d}\mu_1}(1-\mu_1^2)^{1/2}, \end{aligned} \tag{A28}$$

$$B_{1n}^{"} = \lambda^{-1/2}r_1^{-3/2}(-\lambda r_1 K_{n-1/2}(\lambda r_1) - (n+2)K_{n+1/2}(\lambda r_1))P_n^1(\mu_1)(1-\mu_1^2)^{-1/2}, \tag{A29}$$

$$C_{1n}^{"} = -2n(n+2)r_1^{-n-3}\frac{\mathrm{d}P_n^1(\mu_1)}{\mathrm{d}\mu_1}(1-\mu_1^2)^{1/2}, \tag{A30}$$

$$\begin{aligned} A_{2n}^{"} = \lambda^{-1/2}r_1^{-5/2}(&-(2n^2+4n+\lambda^2r_1^2)I_{n+1/2}(\lambda r_1) \\ &+2\lambda r_1 I_{n-1/2}(\lambda r_1))\frac{\mathrm{d}P_n^1(\mu_1)}{\mathrm{d}\mu_1}(1-\mu_1^2)^{1/2}, \end{aligned} \tag{A31}$$

$$B_{2n}^{"} = \lambda^{-1/2}r_1^{-3/2}(\lambda r_1 I_{n-1/2}(\lambda r_1) - (n+2)I_{n+1/2}(\lambda r_1))P_n^1(\mu_1)(1-\mu_1^2)^{-1/2}, \tag{A32}$$

$$C_{2n}^{"} = -2(n+1)(n-1)r_1^{n-2}\frac{\mathrm{d}P_n^1(\mu_1)}{\mathrm{d}\mu_1}(1-\mu_1^2)^{1/2}, \tag{A33}$$

doi:10.6342/NTU202502609

$$A_{1n}^{***} = -2\frac{(n+1)(n-1)}{n} r_1^{-n-1} P_n^1(\mu_1)(1-\mu_1^2)^{-1/2}, \tag{A34}$$

$$B_{1n}^{***} = -(n+2) r_1^{-n-2} \frac{\mathrm{d}P_n^1(\mu_1)}{\mathrm{d}\mu_1}(1-\mu_1^2)^{1/2}, \tag{A35}$$

$$C_{1n}^{***} = -2(n+2) r_1^{-n-3} P_n^1(\mu_1)(1-\mu_1^2)^{-1/2}, \tag{A36}$$

$$A_{2n}^{***} = r_2^{n+1}[\Gamma_4^{(2)} + \Gamma_5^{(2)} - n r_1^{-1} f^{(1)} P_n^1(\mu_2)(1-\mu_1^2)^{-1/2}], \tag{A37}$$

$$\begin{aligned} B_{2n}^{***} = r_2^{n}\{ & r_1^{-1} f^{(2)} P_n^1(\mu_2)(1-\mu_1^2)^{-1/2}(1-\mu_2^2)^{-1/2} \\ & + (n r_2^{-1}\frac{\partial r_2}{\partial r_1} - r_1^{-1})\frac{\mathrm{d}P_n^1(\mu_2)}{\mathrm{d}\mu_2}(1-\mu_2^2)^{1/2} \\ & + \frac{\partial \theta_2}{\partial r_1}[\frac{\mathrm{d}P_n^1(\mu_2)}{\mathrm{d}\mu_2}\mu_2 - \frac{\mathrm{d}^2 P_n^1(\mu_2)}{\mathrm{d}\mu_2^2}(1-\mu_2^2)]\}, \end{aligned} \tag{A38}$$

$$C_{2n}^{***} = r_2^{n-1}[\Gamma_4^{(1)} + \Gamma_5^{(1)} - n r_1^{-1} f^{(1)} P_n^1(\mu_2)(1-\mu_1^2)^{-1/2}], \tag{A39}$$

$$\begin{aligned} A_{1n}^{'''} = \lambda^{-1/2} r_1^{-5/2}(&-(2n^2+4n+\lambda^2 r_1^2) K_{n+1/2}(\lambda r_1) \\ & -2\lambda r_1 K_{n-1/2}(\lambda r_1)) P_n^1(\mu_1)(1-\mu_1^2)^{-1/2}, \end{aligned} \tag{A40}$$

$$B_{1n}^{'''} = \lambda^{-1/2} r_1^{-3/2}(-\lambda r_1 K_{n-1/2}(\lambda r_1) - (n+2) K_{n+1/2}(\lambda r_1))\frac{\mathrm{d}P_n^1(\mu_1)}{\mathrm{d}\mu_1}(1-\mu_1^2)^{1/2}, \tag{A41}$$

$$C_{1n}^{'''} = -2n(n+2) r_1^{-n-3} P_n^1(\mu_1)(1-\mu_1^2)^{-1/2}, \tag{A42}$$

$$\begin{aligned} A_{2n}^{'''} = \lambda^{-1/2} r_1^{-5/2}(&-(2n^2+4n+\lambda^2 r_1^2) I_{n+1/2}(\lambda r_1) \\ & +2\lambda r_1 I_{n-1/2}(\lambda r_1)) P_n^1(\mu_1)(1-\mu_1^2)^{-1/2}, \end{aligned} \tag{A43}$$

$$B_{2n}^{'''} = \lambda^{-1/2} r_1^{-3/2}(\lambda r_1 I_{n-1/2}(\lambda r_1) - (n+2) I_{n+1/2}(\lambda r_1))\frac{\mathrm{d}P_n^1(\mu_1)}{\mathrm{d}\mu_1}(1-\mu_1^2)^{1/2}, \tag{A44}$$

$$C_{2n}^{'''} = -2(n+1)(n-1) r_1^{n-2} P_n^1(\mu_1)(1-\mu_1^2)^{-1/2}, \tag{A45}$$

where the simplified expressions of $\partial r_2 / \partial r_1$, $\partial r_2 / \partial \theta_1$, $\partial \theta_2 / \partial r_1$, and $\partial \theta_2 / \partial \theta_1$ were

doi:10.6342/NTU202502609

given by Lee and Keh (2013b), $f^{(1)}$ and $f^{(2)}$ are given by equation (17),

$$\Gamma_1^{(k)} = [n(n+2k-3)r_2^{-1}(\frac{\partial r_2}{\partial r_1} f^{(2)} + r_1^{-1}\frac{\partial r_2}{\partial \theta_1} f^{(1)}) + n\frac{\partial f^{(2)}}{\partial r_1} + nr_1^{-1}(\frac{\partial f^{(1)}}{\partial \theta_1} - f^{(2)})]P_n^1(\mu_2), \quad \text{(A46)}$$

$$\Gamma_2^{(k)} = [(n+4k-5)r_2^{-1}(r_1^{-1}\frac{\partial r_2}{\partial \theta_1} f^{(2)} - \frac{\partial r_2}{\partial r_1} f^{(1)}) - n\frac{\partial \theta_2}{\partial r_1} f^{(2)} - nr_1^{-1}\frac{\partial \theta_2}{\partial \theta_1} f^{(1)}$$

$$-\frac{n+2k-1}{n+1}(\frac{\partial f^{(1)}}{\partial r_1} - r_1^{-1}\frac{\partial f^{(2)}}{\partial \theta_1} - r_1^{-1} f^{(1)})]\frac{\mathrm{d}P_n^1(\mu_2)}{\mathrm{d}\mu_2}(1-\mu_2^{\,2})^{1/2}, \quad \text{(A47)}$$

$$\Gamma_3^{(k)} = \frac{n+2k-1}{n+1}(r_1^{-1}\frac{\partial \theta_2}{\partial \theta_1} f^{(2)} - \frac{\partial \theta_2}{\partial r_1} f^{(1)})[\frac{\mathrm{d}P_n^1(\mu_2)}{\mathrm{d}\mu_2}\mu_2 - \frac{\mathrm{d}^2 P_n^1(\mu_2)}{\mathrm{d}\mu_2^{\,2}}(1-\mu_2^{\,2})], \quad \text{(A48)}$$

$$\Gamma_4^{(k)} = \{\frac{n+2k-1}{n+1}[\frac{\partial \theta_2}{\partial r_1}\mu_2(1-\mu_2^{\,2})^{-1/2} + r_1^{-1}] - (n+4k-5)r_2^{-1}\frac{\partial r_2}{\partial r_1}\}P_n^1(\mu_2)(1-\mu_2^{\,2})^{-1/2}, \quad \text{(A49)}$$

$$\Gamma_5^{(k)} = \frac{n+2k-1}{n+1}[\frac{\partial \theta_2}{\partial r_1} - r_1^{-1} f^{(2)}(1-\mu_1^{\,2})^{-1/2}(1-\mu_2^{\,2})^{1/2}]\frac{\mathrm{d}P_n^1(\mu_2)}{\mathrm{d}\mu_2}, \quad \text{(A50)}$$

$$\frac{\partial f^{(1)}}{\partial r_1} = -\frac{\partial \theta_2}{\partial r_1} f^{(2)}, \qquad \frac{\partial f^{(1)}}{\partial \theta_1} = (1-\frac{\partial \theta_2}{\partial \theta_1}) f^{(2)}, \quad \text{(A51)}$$

$$\frac{\partial f^{(2)}}{\partial r_1} = \frac{\partial \theta_2}{\partial r_1} f^{(1)}, \qquad \frac{\partial f^{(2)}}{\partial \theta_1} = (\frac{\partial \theta_2}{\partial \theta_1} - 1) f^{(1)}. \quad \text{(A52)}$$

doi:10.6342/NTU202502609

Appendix B

Translation of a Composite Sphere in an Eccentric Spherical Cavity along Their Common Diameter

B.1 Introduction

The objective of this appendix is to obtain a theoretical solution for the quasi-steady slow translation of a soft spherical particle in a non-concentric spherical cavity along their common diameter. A boundary collocation method (Keh and Lee 2010, Chou and Keh 2022) will be used to solve the creeping flow equations applicable to this system, and the wall-corrected hydrodynamic drag exerted on the particle will be obtained in many cases. The drag results reveal some interesting features of the influence of the cavity wall on soft particle motion.

doi:10.6342/NTU202502609

B.2 Analysis

As shown in Fig. B1, we consider the quasi-steady flow caused by a soft spherical particle of radius b translating with a velocity U in an incompressible Newtonian fluid inside an eccentric spherical cavity of radius c along their common diameter (z axis). Here, (ρ,ϕ,z) and (r_2,θ_2,ϕ) represent the circular cylindrical and spherical coordinate systems, respectively, with their origins attached to the cavity center. The soft particle has a hard core of radius a and a porous layer of thickness $b-a$. The center of the particle is situated at a distance d from the cavity center instantaneously. The purpose is to determine the correction for the hydrodynamic drag experienced by the particle because of the existence of the cavity.

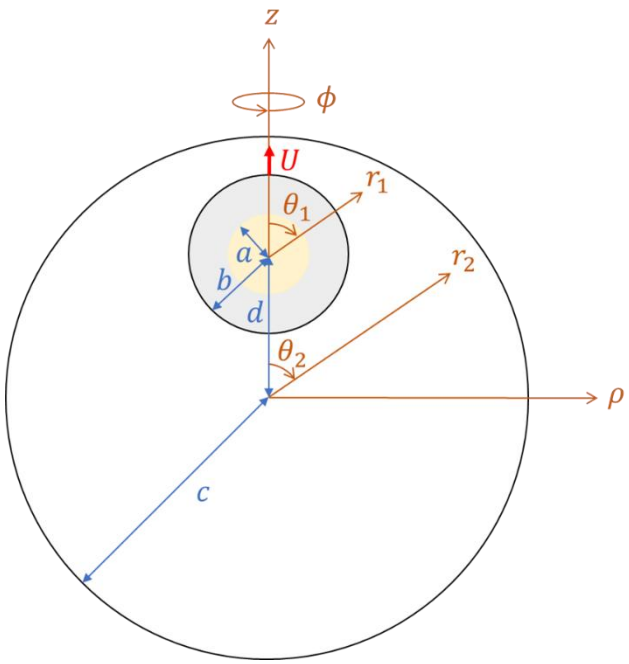

Fig. B1. A soft spherical particle translating inside a spherical cavity along their common diameter.

doi:10.6342/NTU202502609

Owing to low Reynolds number, the fluid motion is governed by the Brinkman (inside the porous surface layer) and Stokes (outside the soft sphere) equations for the axisymmetric creeping flow,

$$(E^2-\lambda^2)E^2\hat{\Psi}=0 \qquad (a\le r_1\le b), \tag{B1}$$

$$E^2(E^2\Psi)=0 \qquad (r_1\ge b \ \text{ and } \ r_2\le c), \tag{B2}$$

where (r_1,θ_1,ϕ) is the spherical coordinate system based on the center of the soft particle, λ^{-1} is the permeation length or square root of the fluid permeability in the porous layer, $\hat{\Psi}$ and Ψ are stream functions of the flow in the porous layer and external flow, respectively, related to their nontrivial velocity components $(\hat{v}_{r_i},\hat{v}_{\theta_i})$ and (v_{r_i},v_{θ_i}) in spherical coordinates by

$$(\hat{v}_{r_i},v_{r_i})=-\frac{1}{r_i^2\sin\theta_i}\frac{\partial(\hat{\Psi},\Psi)}{\partial\theta_i}, \qquad (\hat{v}_{\theta_i},v_{\theta_i})=\frac{1}{r_i\sin\theta_i}\frac{\partial(\hat{\Psi},\Psi)}{\partial r_i}, \tag{B3}$$

the Stokes operator

$$E^2=\frac{\partial^2}{\partial r_i^2}+\frac{\sin\theta_i}{r_i^2}\frac{\partial}{\partial\theta_i}\left(\frac{1}{\sin\theta_i}\frac{\partial}{\partial\theta_i}\right), \tag{B4}$$

and $i=1$ or 2.

The boundary conditions for the fluid flow are

$$r_1=a: \qquad \hat{\mathbf{v}}_{r_1}=\hat{\mathbf{v}}_{\theta_1}=\mathbf{O}, \tag{B5}$$

$$r_1=b: \qquad v_{r_1}=\hat{v}_{r_1}, \qquad v_{\theta_1}=\hat{v}_{\theta_1}, \tag{B6a}$$

doi:10.6342/NTU202502609

$$\tau_{r_1\theta_1} = \hat{\tau}_{r_1\theta_1}, \qquad \tau_{r_1r_1} - p = \hat{\tau}_{r_1r_1} - \hat{p}, \tag{B6b}$$

$$r_2 = c: \qquad v_{r_2} = -U\cos\theta_2, \qquad v_{\theta_2} = U\sin\theta_2. \tag{B7}$$

Here, $(\hat{\tau}_{r_1\theta_1}, \hat{\tau}_{r_1r_1})$ and $(\tau_{r_1\theta_1}, \tau_{r_1r_1})$ are the nontrivial stress components in the spherical coordinates (r_1, θ_1, ϕ) for the flow in the porous surface layer and external flow, respectively, $\hat{p}$ and p are the matching pressure profiles, and Eqs. (B5)-(B7) take a reference frame translating with the soft particle. For axisymmetric motions with the effective viscosity of the fluid in the porous layer equal to the bulk fluid viscosity (Koplik *et al* 1983, Masliyah *et al* 1987) and satisfying Eq. (B6a) simultaneously, the boundary condition (B6b) is equivalent to (Chen 1998)

$$r_1 = b: \qquad \frac{\partial v_{\theta_1}}{\partial r_1} = \frac{\partial \hat{v}_{\theta_1}}{\partial r_1}, \qquad p = \hat{p} \ \ (\text{or} \ \ \tau_{r_1r_1} = \hat{\tau}_{r_1r_1}). \tag{B8}$$

We can express the stream functions as (Keh and Lee 2010, Chen and Ye 2000)

$$\hat{\Psi} = \sum_{n=2}^{\infty} \{A_{1n} r_1^{\,n} + B_{1n} r_1^{\,-n+1} + [C_{1n} I_{n-1/2}(\lambda r_1) + D_{1n} K_{n-1/2}(\lambda r_1)](\lambda r_1)^{1/2}\} G_n^{-1/2}(\cos\theta_1), \tag{B9}$$

$$\Psi = \sum_{n=2}^{\infty} [(A_{2n} r_2^{\,n} + C_{2n} r_2^{\,n+2}) G_n^{-1/2}(\cos\theta_2) + (B_{2n} r_1^{\,-n+1} + D_{2n} r_1^{\,-n+3}) G_n^{-1/2}(\cos\theta_1)], \tag{B10}$$

where I_n and K_n are the modified Bessel functions of the first and second kinds of order n, respectively, and $G_n^{-1/2}$ is the Gegenbauer polynomial of the first kind of order n and degree $-1/2$. The unknown coefficients A_{in}, B_{in}, C_{in}, and D_{in} ($i = 1$ or 2) will be determined using Eqs. (B5)-(B7). When constructing the solution (B10), the

doi:10.6342/NTU202502609

general solutions of Eq. (B2) in the two spherical coordinate systems can be superimposed due to the linearity of this equation.

Application of Eq. (B3) to Eqs. (B9) and (B10) leads to the components of fluid velocities $(\hat{v}_\rho, \hat{v}_z)$ and (v_ρ, v_z) for the flow inside the porous layer and external flow, respectively, in circular cylindrical coordinates as

$$\hat{v}_\rho = \sum_{n=2}^{\infty} [A_{1n} A_n'(r_1, \theta_1) + B_{1n} B_n'(r_1, \theta_1) + C_{1n} \gamma_n'(r_1, \theta_1) + D_{1n} \delta_n'(r_1, \theta_1)], \tag{B11a}$$

$$\hat{v}_z = \sum_{n=2}^{\infty} [A_{1n} A_n''(r_1, \theta_1) + B_{1n} B_n''(r_1, \theta_1) + C_{1n} \gamma_n''(r_1, \theta_1) + D_{1n} \delta_n''(r_1, \theta_1)]; \tag{B11b}$$

$$v_\rho = \sum_{n=2}^{\infty} [A_{2n} A_n'(r_2, \theta_2) + C_{2n} C_n'(r_2, \theta_2) + B_{2n} B_n'(r_1, \theta_1) + D_{2n} D_n'(r_1, \theta_1)], \tag{B12a}$$

$$v_z = \sum_{n=2}^{\infty} [A_{2n} A_n''(r_2, \theta_2) + C_{2n} C_n''(r_2, \theta_2) + B_{2n} B_n''(r_1, \theta_1) + D_{2n} D_n''(r_1, \theta_1)], \tag{B12b}$$

where A_n', A_n'', B_n', B_n'', C_n', C_n'', D_n', D_n'', γ_n', γ_n'', δ_n', and δ'' are functions of spherical coordinates (r, θ) defined by Eqs. (C1)-(C12) in Appendix C. Applying boundary conditions (B5)-(B7) to Eqs. (B11) and (B12), we obtain

$$\sum_{n=2}^{\infty} [A_{1n} A_n'(a, \theta_1) + B_{1n} B_n'(a, \theta_1) + C_{1n} \gamma_n'(a, \theta_1) + D_{1n} \delta_n'(a, \theta_1)] = 0, \tag{B13a}$$

$$\sum_{n=2}^{\infty} [A_{1n} A_n''(a, \theta_1) + B_{1n} B_n''(a, \theta_1) + C_{1n} \gamma_n''(a, \theta_1) + D_{1n} \delta_n''(a, \theta_1)] = 0; \tag{B13b}$$

$$\sum_{n=2}^{\infty} \{[A_{2n} A_n'(r_2, \theta_2) + C_{2n} C_n'(r_2, \theta_2)]_{r_1=b} + B_{2n} B_n'(b, \theta_1) + D_{2n} D_n'(b, \theta_1)$$

doi:10.6342/NTU202502609

$$-A_{1n}A_n'(b,\theta_1)-B_{1n}B_n'(b,\theta_1)-C_{1n}\gamma_n'(b,\theta_1)-D_{1n}\delta_n'(b,\theta_1)\}=0\,, \quad \text{(B14a)}$$

$$\sum_{n=2}^{\infty}\{[A_{2n}A_n''(r_2,\theta_2)+C_{2n}C_n''(r_2,\theta_2)]_{r_1=b}+B_{2n}B_n''(b,\theta_1)+D_{2n}D_n''(b,\theta_1)$$

$$-A_{1n}A_n''(b,\theta_1)-B_{1n}B_n''(b,\theta_1)-C_{1n}\gamma_n''(b,\theta_1)-D_{1n}\delta_n''(b,\theta_1)\}=0\,, \quad \text{(B14b)}$$

$$\sum_{n=2}^{\infty}\{[A_{2n}A_n^{*}(r_2,\theta_2)+C_{2n}C_n^{*}(r_2,\theta_2)]_{r_1=b}+B_{2n}B_n^{*}(b,\theta_1)+D_{2n}D_n^{*}(b,\theta_1)$$

$$-A_{1n}A_n^{*}(b,\theta_1)-B_{1n}B_n^{*}(b,\theta_1)-C_{1n}\gamma_n^{*}(b,\theta_1)-D_{1n}\delta_n^{*}(b,\theta_1)\}=0\,, \quad \text{(B14c)}$$

$$\sum_{n=2}^{\infty}\{[A_{2n}A_{2n}^{**}(r_2,\theta_2)+C_{2n}C_n^{**}(r_2,\theta_2)]_{r_1=b}+B_{2n}B_{2n}^{**}(b,\theta_1)+D_{2n}D_n^{**}(b,\theta_1)$$

$$-A_{1n}A_{1n}^{**}(b,\theta_1)-B_{1n}B_{1n}^{**}(b,\theta_1)-C_{1n}\gamma_n^{**}(b,\theta_1)-D_{1n}\delta_n^{**}(b,\theta_1)\}=0\,; \quad \text{(B14d)}$$

$$\sum_{n=2}^{\infty}\{A_{2n}A_n^{***}(c,\theta_2)+C_{2n}C_n^{***}(c,\theta_2)+[B_{2n}B_n^{***}(r_1,\theta_1)+D_{2n}D_n^{***}(r_1,\theta_1)]_{r_2=c}\}=-U\,, \quad \text{(B15a)}$$

$$\sum_{n=2}^{\infty}\{A_{2n}A_n^{****}(c,\theta_2)+C_{2n}C_n^{****}(c,\theta_2)+[B_{2n}B_n^{****}(r_1,\theta_1)+D_{2n}D_n^{****}(r_1,\theta_1)]_{r_2=c}\}=-U\,, \quad \text{(B15b)}$$

where A_n^{*}, A_{1n}^{**}, A_{2n}^{**}, A_n^{***}, A_n^{****}, B_n^{*}, B_{1n}^{**}, B_{2n}^{**}, B_n^{***}, B_n^{****}, C_n^{*}, C_n^{**}, C_n^{***}, C_n^{****}, D_n^{*}, D_n^{**}, D_n^{***}, D_n^{****}, γ_n^{*}, γ_n^{**}, δ_n^{*}, and δ_n^{**} are functions of (r,θ) defined by Eqs. (C13)-(C34).

To exactly satisfy the conditions in Eqs. (B13)-(B15), solutions of the whole infinite unknown constants A_{in}, B_{in}, C_{in}, and D_{in} are required. But, the collocation technique (Keh and Lee 2010, Chou and Keh 2022) enforces boundary conditions at a limited number of discrete points on the longitudinal semicircle of each of the spherical surfaces

doi:10.6342/NTU202502609

(from $\theta_j = 0$ to $\theta_j = \pi$ at $r_1 = a$, $r_1 = b$, and $r_2 = c$) and truncates the infinite series in Eqs. (B9)-(B12) to finite series. If the longitudinal semicircle is approximated by N discrete points satisfying the conditions in Eqs. (B5)-(B7), then the infinite series in Eqs. (B9)-(B12) are truncated after N terms, resulting in $8N$ linear algebraic equations in the truncated form of Eqs. (B13)-(B15). These equations can be solved numerically to produce the $8N$ unknowns A_{in}, B_{in}, C_{in}, and D_{in} required for the truncated Eqs. (B9)-(B12). Once these unknowns are solved for a sufficiently large number of N, the fluid velocity can be fully obtained. Details of the boundary collocation scheme are given in a previous paper on the translational motion of a hard spherical particle in a cavity (Keh and Lee 2010).

The drag force exerted by the external fluid on the soft particle (in the opposite direction of U) can be determined from (Happel and Brenner 1983)

$$F = 4\pi\eta D_{22}, \tag{B16}$$

where η is viscosity of the fluid. The previous equation indicates that only the lowest-order constant D_{22} contributes to the hydrodynamic force acting on the particle. If the soft sphere is located at the center of the spherical cavity ($d = 0$), D_{22} can be obtained analytically as Eq. (C35).

When the porous layer of the soft particle vanishes, it reduces to a hard particle of radius $a = b$, Eqs. (B1), (B5), (B6b), (B8), (B9), (B11), (B13) and (B14c,d) are trivial,

doi:10.6342/NTU202502609

$\hat{v}_\rho = \hat{v}_z = 0$, $A_{1n} = B_{1n} = C_{1n} = D_{1n} = 0$, and just Eqs. (B14a,b) and (B15) are needed to be solved for the $4N$ unknown constants A_{2n}, B_{2n}, C_{2n}, and D_{2n}. When the hard core disappears ($a = 0$), the soft sphere reduces to a porous particle of radius b, Eqs. (B5) and (B13) are trivial, $B_{1n} = D_{1n} = 0$, and just Eqs. (B14) and (B15) are needed for the $6N$ unknowns A_{1n}, C_{1n}, A_{2n}, B_{2n}, C_{2n}, and D_{2n}.

In the limiting case of $b/c = 0$, the soft sphere is unconfined and Eq. (B16) can be expressed analytically as Eq. (1). For the cases of $a = b$ and $a = 0$, Eq. (1) becomes Stokes' law ($F_0 = 6\pi\eta bU$) for a hard sphere and corresponding result for a porous sphere, respectively. In the limits $\lambda b \to \infty$ (impermeable in the porous surface layer of the particle) and $\lambda b = 0$ (completely permeable in the porous surface layer), Eq. (1) again simplifies to Stokes' law for hard spheres of radii b and a, respectively.

doi:10.6342/NTU202502609

B.3 Results and Discussion

Results of the hydrodynamic drag force acting on a soft sphere translating inside an eccentric spherical cavity, obtained with good convergence by using the boundary collocation technique described in the previous section for various values of the ratios of the core-to-particle radii a/b, particle-to-cavity radii b/c, distance between the centers to radius difference of the cavity and particle $d/(c-b)$, and particle radius to porous layer permeation length λb, are presented for cases of porous sphere ($a=0$) and general soft sphere in Tables B1 and B2, respectively. The drag force F_0 acting on an identical particle in the unbounded fluid given by Eq. (1) is used to normalize the cavity-corrected value F. These results converge to at least the significant digits as given in the tables and agree well with the available analytical solution in the concentric limit $d/(c-b)=0$ given in Appendix C. Also, our results in the limit $b/c \to 0$ (vanishing cavity wall curvature compared with the particle) but finite in $b/(c-d)$ are in good agreement with the results for a soft spherical particle translating perpendicular to a large plane wall obtained by Chen and Ye (2000). In the limit $\lambda b \to \infty$ (or $a=b$), our results agree well with those (Keh and Lee 2010) obtained for a hard sphere translating in a corresponding cavity. $F/F_0=1$ as $b/(c-d)=0$ (the cavity wall is far away from the particle) as expected, irrespective of the other parameters.

doi:10.6342/NTU202502609

Table B1 The normalized drag force F/F_0 experienced by a porous sphere ($a = 0$) translating inside a spherical cavity at different values of $d/(c-b)$, b/c, and λb.

$\frac{d}{(c-b)}$	b/c	F/F_0				
		$\lambda b = 0.1$	$\lambda b = 1$	$\lambda b = 10$	$\lambda b = 100$	$\lambda b = 500$
0.25	0.1	0.9949	1.0380	1.2619	1.3015	1.3048
	0.2	0.9702	1.0569	1.6570	1.7931	1.8046
	0.3	0.9626	1.0890	2.2845	2.6428	2.6738
	0.4	0.9673	1.1303	3.3190	4.2244	4.3053
	0.5	0.9766	1.1728	5.0786	7.4727	7.6958
	0.6	0.9869	1.2108	8.0957	15.1128	15.8189
	0.7	0.9953	1.2397	12.9569	37.0789	39.9815
	0.8	1.0004	1.2572	19.2043	1.244E2	1.447E2
	0.9	1.0023	1.2643	23.9350	6.971E2	1.195E3
	0.95	1.0018	1.2652	24.8577	1.692E3	7.847E3
	0.975	1.0023	1.2649	24.9698	2.025E3	2.702E4
	0.99	1.0026	1.2654	25.0226	2.212E3	4.747E4
	0.999	1.0027	1.2655	25.0247	2.245E3	5.564E4
0.5	0.1	0.9901	1.0419	1.3253	1.3778	1.3821
	0.2	0.9389	1.0379	1.8007	1.9933	2.0100
	0.3	0.8681	1.0007	2.5106	3.0559	3.1058
	0.4	0.8634	1.0237	3.6576	5.0423	5.1760
	0.5	0.9022	1.0925	5.5773	9.1351	9.5057
	0.6	0.9435	1.1622	8.7466	18.7607	19.9314
	0.7	0.9755	1.2169	13.5844	46.2215	51.0323
	0.8	0.9943	1.2500	19.4783	1.521E2	1.857E2
	0.9	1.0014	1.2631	23.9276	7.604E2	1.522E3
	0.95	1.0023	1.2649	24.8262	1.600E3	9.517E3
	0.975	1.0010	1.2633	24.8767	1.756E3	1.958E4
	0.99	1.0021	1.2647	24.9957	2.147E3	3.790E4
	0.999	1.0027	1.2654	25.0246	2.245E3	5.564E4

doi:10.6342/NTU202502609

Table B2 The normalized drag force F/F_0 experienced by a soft sphere with $\lambda b = 1$ translating inside a spherical cavity at different values of $d/(c-b)$, b/c, and a/b.

$\frac{d}{(c-b)}$	b/c	F/F_0		
		$a/b = 0.5$	$a/b = 0.8$	$a/b = 0.95$
0.25	0.1	1.1387	1.2304	1.2858
	0.2	1.2976	1.5592	1.7389
	0.3	1.5105	2.0622	2.5003
	0.4	1.7973	2.8642	3.8672
	0.5	2.1822	4.2100	6.5427
	0.6	2.7002	6.6206	12.4338
	0.7	3.3984	11.3193	27.8263
	0.8	4.3408	21.5831	80.8279
	0.9	5.6261	48.0522	3.924E2
	0.95	6.4505	78.1032	1.327E3
	0.975	6.9168	1.021E2	2.846E3
	0.99	7.2290	1.224E2	5.793E3
	0.999	7.4251	1.369E2	9.589E3
0.5	0.1	1.1668	1.2842	1.3569
	0.2	1.3269	1.6664	1.9150
	0.3	1.4769	2.1951	2.8323
	0.4	1.7280	3.0461	4.4755
	0.5	2.1288	4.5028	7.6832
	0.6	2.6887	7.1133	14.6867
	0.7	3.4357	12.1532	32.7173
	0.8	4.4057	22.8894	93.2114
	0.9	5.6672	49.4743	4.310E2
	0.95	6.4648	78.8504	1.351E3
	0.975	6.9173	1.009E2	2.153E3
	0.99	7.2224	1.221E2	5.328E3
	0.999	7.4251	1.369E2	9.587E3

doi:10.6342/NTU202502609

The normalized drag force F/F_0 of a porous sphere ($a=0$) translating axisymmetrically within a non-concentric spherical cavity is plotted against the parameters b/c, $d/(c-b)$, and λb in Figs. B2-B4, respectively. For fixed values of $d/(c-b)$ and b/c, F/F_0 increases monotonically with a decrease in permeability or an increase in λb from unity (with $F=F_0=0$) at $\lambda b=0$ to a finite value (or infinity at the limit $b/c=1$ where the particle seals the cavity) as $\lambda b\to\infty$, as illustrated in Table B1 and Figs. B2a, B3b, B4a, and B4b. F/F_0 changes weakly with $d/(c-b)$ and b/c (less than 27% for all cases with $b/c\le 0.999$) as $\lambda b\le 1$. When b/c and $d/(c-b)$ are not close to unity, the normalized force on a porous particle with $\lambda b>100$ approaches to that with $\lambda b\to\infty$ (a porous sphere of little permeability performs as a hard sphere), but when the porous sphere is near the wall, the difference can become significant.

doi:10.6342/NTU202502609

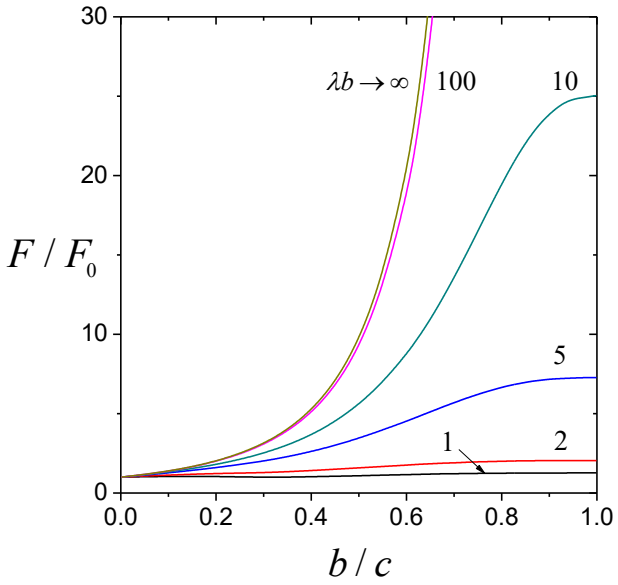

(a)

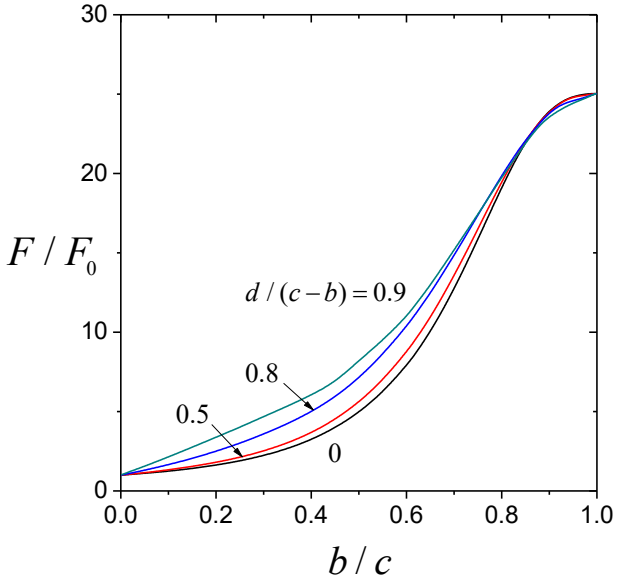

(b)

Fig. B2. Normalized drag force F/F_0 of a porous sphere ($a = 0$) translating inside a spherical cavity versus the ratio of particle-to-cavity radii b/c: (a) $d/(c-b) = 1/2$; (b) $\lambda b = 10$.

doi:10.6342/NTU202502609

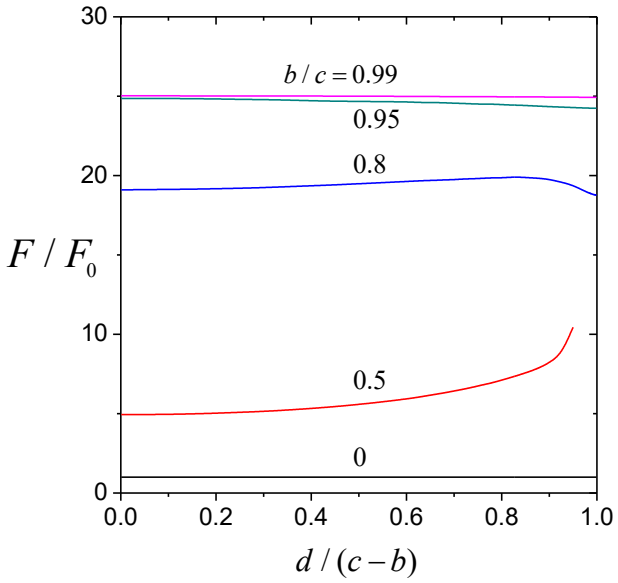

(a)

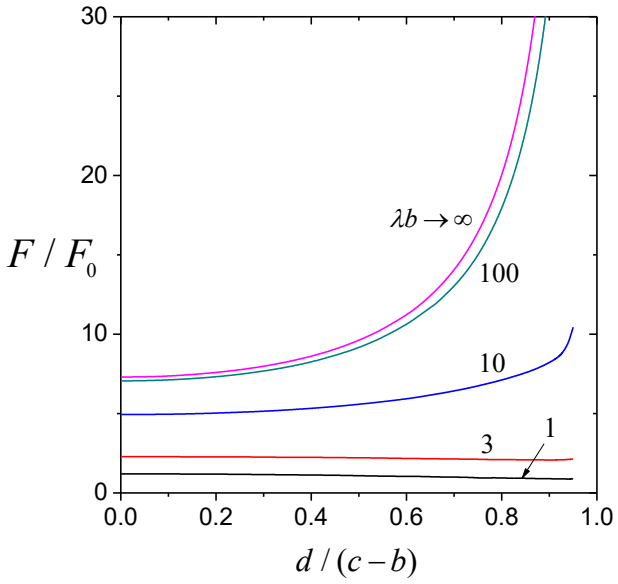

(b)

Fig. B3. Normalized drag force F/F_0 of a porous sphere ($a = 0$) translating inside a spherical cavity versus the eccentricity parameter $d/(c-b)$: (a) $\lambda b = 10$; (b) $b/c = 1/2$.

doi:10.6342/NTU202502609

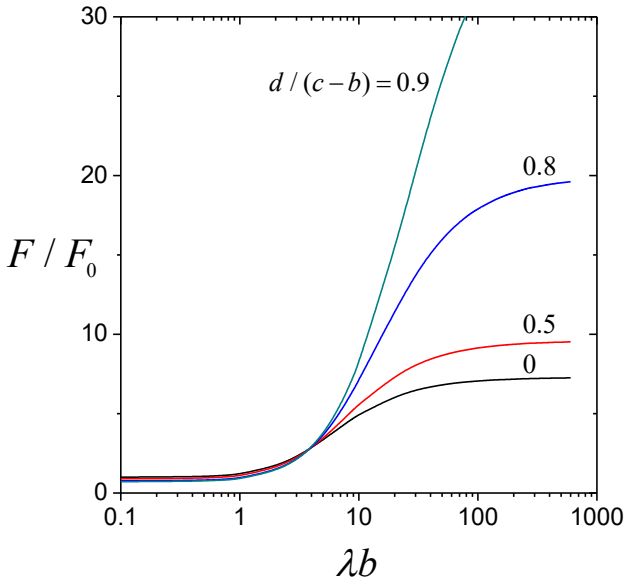

(a)

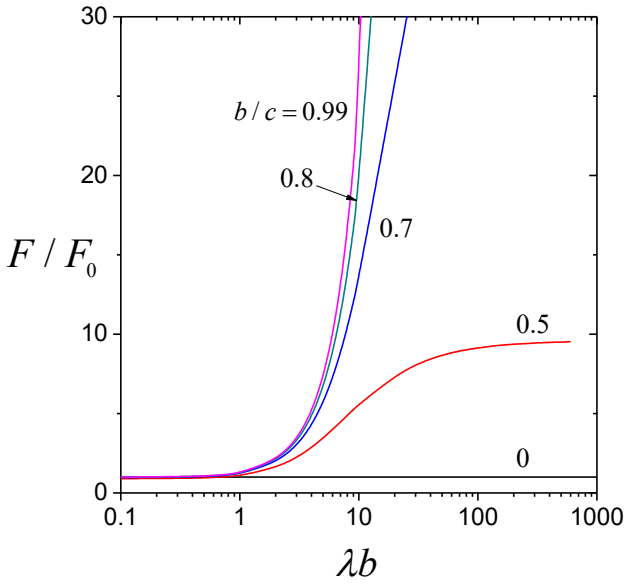

(b)

Fig. B4. Normalized drag force F/F_0 of a porous sphere ($a = 0$) translating inside a spherical cavity versus the shielding parameter λb: (a) $b/c = 1/2$; (b) $d/(c-b) = 1/2$.

doi:10.6342/NTU202502609

For given values of λb and $d/(c-b)$, as illustrated in Table B1 and Figs. B2a, B2b, B3a, and B4b, the normalized force F/F_0 acting on a porous sphere generally is an increasing function of the ratio of the particle-to-cavity radii b/c from unity at $b/c=0$ to a finite value (or infinity if $\lambda b \to \infty$) at $b/c=1$, because the closer the cavity wall to the particle surface, the stronger the hydrodynamic hindrance effect of the wall. Unexpectedly, when $d/(c-b)$ is not near zero (the particle eccentricity within the cavity is not negligible) and λb is smaller than about 2 (the porous sphere is relatively permeable), F/F_0 may not be a monotonic function of b/c, and reach a minimum either greater or less than unity at medium values of b/c (that is, the existence of a confinement wall can decrease the hydrodynamic force on a porous sphere, and this counter-intuitive behavior seems to be caused by the approximations in the porous particle that the volume-averaged superficial velocity of the local fluid is used and its effective viscosity is equal to the bulk fluid viscosity (Koplik *et al* 1983)). The dependence of F/F_0 on b/c disappears at the limit $\lambda b=0$ but is strong when λb is large.

For specified values of b/c and λb, the normalized force F/F_0 generally increases with increasing $d/(c-b)$, the eccentricity parameter, from one finite value in the concentric situation $d/(c-b)=0$ to another at the contact limit of particle and cavity surfaces $d/(c-b)=1$, as shown in Table B1 and Figs. B2b, B3a, B3b, and B4a.

doi:10.6342/NTU202502609

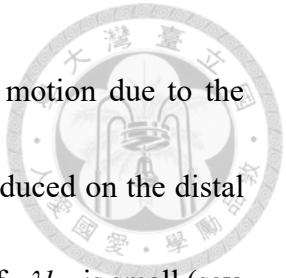

These results indicate that the hydrodynamic hindrance of particle motion due to the proximity of the cavity wall is enhanced on the proximal side and reduced on the distal side of the particle, with an enhanced net effect. But, when the value of λb is small (say, less than about 3) or b/c is large (say, greater than about 0.8), F/F_0 may decrease slightly (even to less than unity) as $d/(c-b)$ increases. The variation of F/F_0 with $d/(c-b)$ vanishes at the limits $\lambda b = 0$ and $b/c = 0$ but is obvious when the value of λb is large.

Having realized the hydrodynamic effects of the non-concentric cavity on a translating porous particle, we can examine the general case of a translating soft particle. In Figs. B5-B8 and Table B2, the normalized force F/F_0 on a soft spherical particle within the cavity is shown as functions of the particle-to-cavity radius ratio b/c, core-to-particle radius ratio a/b, shielding parameter λb, and eccentricity parameter $d/(c-b)$, respectively. Likewise, F/F_0 is a monotonically increasing function of λb from a constant at $\lambda b = 0$ to a finite value (or infinity at the limit $b/c = 1$) as $\lambda b \to \infty$, generally increases with b/c from unity at $b/c = 0$ to a finite value (or infinity in the limit $\lambda b \to \infty$) at $b/c = 1$, and generally rises with increasing $d/(c-b)$ from one finite value in the concentric situation $d/(c-b) = 0$ to another at the contact limit $d/(c-b) = 1$, keeping other parameters unchanged. When the value of a/b is small,

doi:10.6342/NTU202502609

$d/(c-b)$ is not near zero, and λb is smaller than about 2, F/F_0 may first decrease as b/c increases from unity at $b/c=0$, reach a minimum with $F/F_0<1$, and then rise with further increase of b/c up to a value larger than unity at $b/c=1$, as shown in Fig. B6 and Table B2. In addition, when the values of λb and a/b are small (such as less than 3 and 0.5, respectively) F/F_0 may decrease slightly (even to less than unity) as $d/(c-b)$ increases, as illustrated in Table B2 and Figs. B5, B7, and B8.

doi:10.6342/NTU202502609

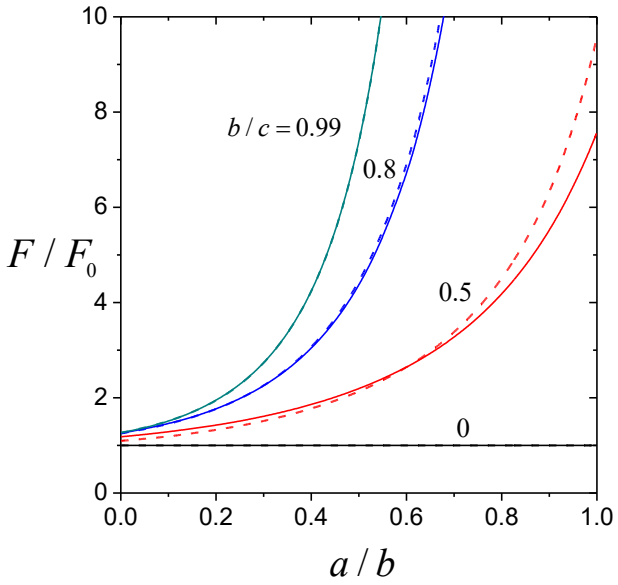

Fig. B5. Normalized drag force F/F_0 of a soft spherical particle translating inside a spherical cavity versus the ratio of core-to-particle radii a/b: (a) $\lambda b = 1$; (b) $b/c = 1/2$. The solid and dashed curves denote $d/(c-b) = 1/5$ and $d/(c-b) = 1/2$, respectively.

doi:10.6342/NTU202502609

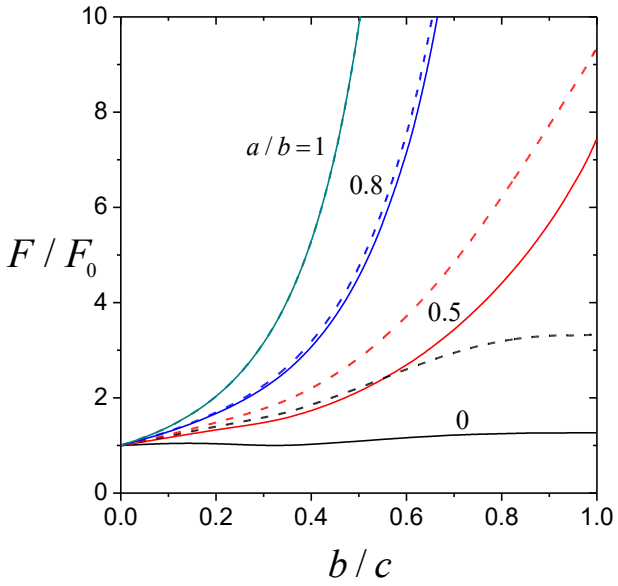

Fig. B6. Normalized drag force F/F_0 of a soft sphere translating inside a spherical cavity with $d/(c-b) = 1/2$ versus the ratio of core-to-particle radii b/c. The solid and dashed curves denote $\lambda b = 1$ and $\lambda b = 3$, respectively.

doi:10.6342/NTU202502609

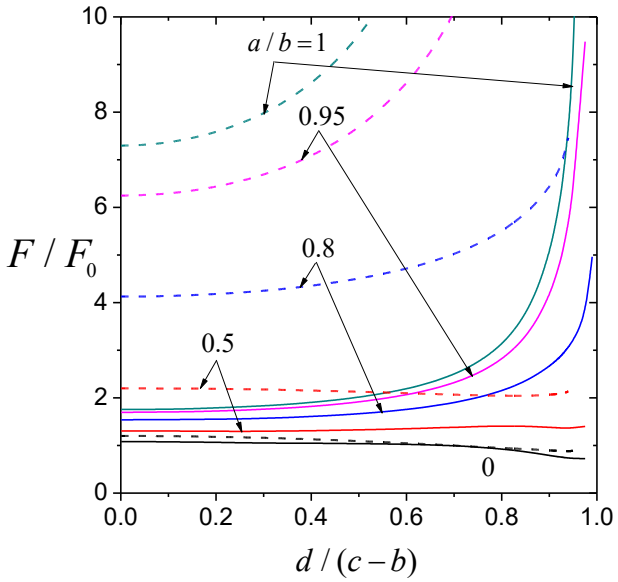

Fig. B7. Normalized drag force F/F_0 of a soft sphere translating inside a spherical cavity with $\lambda b = 1$ versus the eccentricity parameter $d/(c-b)$. The solid and dashed curves denote $b/c = 1/5$ and $b/c = 1/2$, respectively.

doi:10.6342/NTU202502609

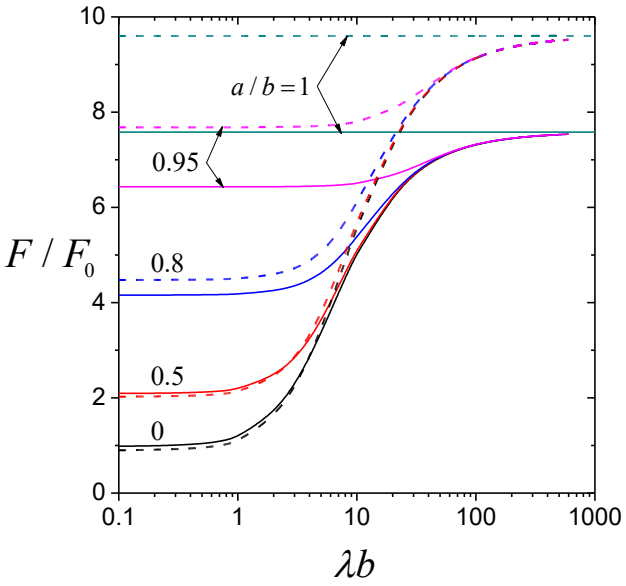

Fig. B8. Normalized drag force F/F_0 of a soft sphere translating inside a spherical cavity with $b/c = 1/2$ versus the shielding parameter λb. The solid and dashed curves denote $d/(c-b) = 1/5$ and $d/(c-b) = 1/2$, respectively.

doi:10.6342/NTU202502609

For fixed values of λb, $d/(c-b)$, and b/c, Figs. B5-B8 and Table B2 show that the normalized force F/F_0 on a translating soft sphere within a spherical cavity monotonically increases with a rise in the ratio of core-to-particle radii a/b, in which the cases of $a/b=0$ and $a/b=1$ denote porous particle and solid particle, respectively. That is, for specified particle radius, permeability of the porous layer, and separation from the wall, the force acting on the particle becomes less if the porous surface layer is thicker. All force results of the soft particle fall between the upper and lower bounds of $a/b=1$ and $a/b=0$, respectively. When the porous layer of the soft particle has small to moderate permeability (say. $\lambda b \geq 10$), F/F_0 on the soft particle with a/b less than about 0.8 within a spherical cavity can be well approximated by the normalized force on a porous particle having identical permeability, radius, and eccentricity inside an identical cavity, as illustrated in Figs. B5b and B8. Here, the hard core of the soft sphere barely feels the motion of the fluid and exerts only negligible hindrance. But, this approximation does not apply to surface layers with high permeability.

doi:10.6342/NTU202502609

B.4 Conclusions

In this Appendix, the axially symmetric translation of a soft sphere in a viscous fluid within an eccentric spherical cavity is semi-analytically investigated in the quasi-steady limit of small Reynolds number. A boundary collocation method is used to solve the Brinkman and Stokes equations for the fluid flows inside and outside the porous surface layer of the soft particle, respectively. Numerical results with good convergence for the normalized drag force F/F_0 exerted by the fluid on the particle are obtained for numerous values of the core-to-particle radius ratio a/b, particle-to-cavity radius ratio b/c, ratio of distance between the centers to radius difference of the particle and cavity $d/(c-b)$, and ratio of particle radius to porous layer permeation length λb. The cavity wall effect on the drag force of a translating soft sphere is monotonically increasing functions of a/b and λb. While F/F_0 generally increases with an increase in b/c, a weak minimum (surprisingly, smaller than unity) may occur for the case of low a/b and low λb. This normalized drag force generally increases with an increase in $d/(c-b)$, but for the case of low a/b and low λb, the drag force may decrease slightly with an increase in $d/(c-b)$.

We presented in Section B.3 the solutions for a resistance problem, in which the drag force F acting on the soft sphere undergoing translation inside a spherical cavity is

doi:10.6342/NTU202502609

determined for a given particle velocity U. On the other hand, in a mobility problem, an applied force F acting on the particle is given and the wall-corrected particle velocity U needs to be determined. For the low-Reynolds-number translational motion of a soft sphere inside a cavity along their common diameter considered here, the normalized particle velocity U/U_0 [where U_0 is given by U in Eq. (1) with $F_0 = F$] for a mobility problem is equal to the reciprocal normalized drag force, $(F/F_0)^{-1}$, provided by Tables B1 and B2 and Figs. B2-B8 for its matching resistance problem.

doi:10.6342/NTU202502609

Appendix C

Some Functions in Appendix B

The functions in Eqs. (B11)-(B15) are defined by

$$A_n'(r,\theta) = -r^{n-2}[(n+1)G_{n+1}^{-1/2}(\cos\theta)\csc\theta - (2n-1)G_n^{-1/2}(\cos\theta)\cot\theta], \tag{C1}$$

$$A_n''(r,\theta) = -r^{n-2}[(2n-1)G_n^{-1/2}(\cos\theta) + P_n(\cos\theta)], \tag{C2}$$

$$B_n'(r,\theta) = -(n+1)r^{-n-1}G_{n+1}^{-1/2}(\cos\theta)\csc\theta, \tag{C3}$$

$$B_n''(r,\theta) = -r^{-n-1}P_n(\cos\theta), \tag{C4}$$

$$C_n'(r,\theta) = -r^{n}[(n+1)G_{n+1}^{-1/2}(\cos\theta)\csc\theta - (2n+1)G_n^{-1/2}(\cos\theta)\cot\theta], \tag{C5}$$

$$C_n''(r,\theta) = -r^{n}[(2n+1)G_n^{-1/2}(\cos\theta) + P_n(\cos\theta)], \tag{C6}$$

$$D_n'(r,\theta) = -r^{-n+1}[(n+1)G_{n+1}^{-1/2}(\cos\theta)\csc\theta - 2G_n^{-1/2}(\cos\theta)\cot\theta], \tag{C7}$$

$$D_n''(r,\theta) = -r^{-n+1}[2G_n^{-1/2}(\cos\theta) + P_n(\cos\theta)], \tag{C8}$$

$$\gamma_n'(r,\theta) = \lambda^{1/2}r^{-3/2}[\lambda r I_{n-3/2}(\lambda r)G_n^{-1/2}(\cos\theta)\cot\theta - (n+1)I_{n-1/2}(\lambda r)G_{n+1}^{-1/2}(\cos\theta)\csc\theta], \tag{C9}$$

$$\gamma_n''(r,\theta) = -\lambda^{1/2}r^{-3/2}[\lambda r I_{n-3/2}(\lambda r)G_n^{-1/2}(\cos\theta) + I_{n-1/2}(\lambda r)P_n(\cos\theta)], \tag{C10}$$

$$\delta_n'(r,\theta) = \lambda^{1/2}r^{-3/2}\{K_{n-1/2}(\lambda r)[nG_n^{-1/2}(\cos\theta)\cot\theta - P_{n-1}(\cos\theta)\sin\theta]$$

$$-\lambda r K_{n+1/2}(\lambda r)G_n^{-1/2}(\cos\theta)\cot\theta\}, \tag{C11}$$

$$\delta_n''(r,\theta) = -\lambda^{1/2}r^{-3/2}\{K_{n-1/2}(\lambda r)[nG_n^{-1/2}(\cos\theta) + P_{n-1}(\cos\theta)\cos\theta]$$

$$-\lambda r K_{n+1/2}(\lambda r)G_n^{-1/2}(\cos\theta)\}; \tag{C12}$$

doi:10.6342/NTU202502609

$$A_n^*(r,\theta) = 2n(n-2)r^{n-3}G_n^{-1/2}(\cos\theta)\csc\theta\,, \tag{C13}$$

$$A_{1n}^{**}(r,\theta) = (-2n+4-\frac{\lambda^2 r^2}{n-1})r^{n-3}P_{n-1}(\cos\theta)\,, \tag{C14}$$

$$A_{2n}^{**}(r,\theta) = -2(n-2)r^{n-3}P_{n-1}(\cos\theta)\,, \tag{C15}$$

$$B_n^*(r,\theta) = 2(n^2-1)r^{-n-2}G_n^{-1/2}(\cos\theta)\csc\theta\,, \tag{C16}$$

$$B_{1n}^{**}(r,\theta) = (2n+2+\frac{\lambda^2 r^2}{n})r^{-n-2}P_{n-1}(\cos\theta)\,, \tag{C17}$$

$$B_{2n}^{**}(r,\theta) = 2(n+1)r^{-n-2}P_{n-1}(\cos\theta)\,, \tag{C18}$$

$$C_n^*(r,\theta) = 2(n^2-1)r^{n-1}G_n^{-1/2}(\cos\theta)\csc\theta\,, \tag{C19}$$

$$C_n^{**}(r,\theta) = -2(n-2-\frac{3}{n-1})r^{n-1}P_{n-1}(\cos\theta)\,, \tag{C20}$$

$$D_n^*(r,\theta) = 2n(n-2)r^{-n}G_n^{-1/2}(\cos\theta)\csc\theta\,, \tag{C21}$$

$$D_n^{**}(r,\theta) = 2(n+1-\frac{3}{n})r^{-n}P_{n-1}(\cos\theta)\,, \tag{C22}$$

$$\gamma_n^*(r,\theta) = -\lambda^{1/2}r^{-5/2}[2\lambda r I_{n+1/2}(\lambda r) - (2n^2-4n+\lambda^2 r^2)I_{n-1/2}(\lambda r)]G_n^{-1/2}(\cos\theta)\csc\theta\,, \tag{C23}$$

$$\gamma_n^{**}(r,\theta) = -2\lambda^{1/2}r^{-5/2}[\lambda r I_{n+1/2}(\lambda r) + (n-2)I_{n-1/2}(\lambda r)]P_{n-1}(\cos\theta)\,, \tag{C24}$$

$$\delta_n^*(r,\theta) = \lambda^{1/2}r^{-5/2}[2\lambda r K_{n+1/2}(\lambda r) + (2n^2-4n+\lambda^2 r^2)K_{n-1/2}(\lambda r)]G_n^{-1/2}(\cos\theta)\csc\theta\,, \tag{C25}$$

$$\delta_n^{**}(r,\theta) = 2\lambda^{1/2}r^{-5/2}[\lambda r K_{n+1/2}(\lambda r) - (n-2)K_{n-1/2}(\lambda r)]P_{n-1}(\cos\theta)\,, \tag{C26}$$

$$A_n^{***}(r,\theta) = -r^{n-2}[(n+1)G_{n+1}^{-1/2}(\cos\theta)\sec\theta + P_n(\cos\theta)]\,, \tag{C27}$$

$$B_n^{***}(r,\theta) = B_n''(r,\theta) + B_n'(r,\theta)\tan\theta_2\,, \tag{C28}$$

$$C_n^{***}(r,\theta) = -r^n[(n+1)G_{n+1}^{-1/2}(\cos\theta)\sec\theta + P_n(\cos\theta)]\,, \tag{C29}$$

$$D_n^{***}(r,\theta) = D_n''(r,\theta) + D_n'(r,\theta)\tan\theta_2\,, \tag{C30}$$

doi:10.6342/NTU202502609

$$A_n^{****}(r,\theta) = -r^{n-2}[(2n-1)G_n^{-1/2}(\cos\theta)\csc^2\theta - (n+1)G_{n+1}^{-1/2}(\cos\theta)\csc\theta\cot\theta + P_n(\cos\theta)], \quad \text{(C31)}$$

$$B_n^{****}(r,\theta) = B_n''(r,\theta) - B_n'(r,\theta)\cot\theta_2, \quad \text{(C32)}$$

$$C_n^{****}(r,\theta) = -r^{n}[(2n+1)G_n^{-1/2}(\cos\theta)\csc^2\theta - (n+1)G_{n+1}^{-1/2}(\cos\theta)\csc\theta\cot\theta + P_n(\cos\theta)], \quad \text{(C33)}$$

$$D_n^{****}(r,\theta) = D_n''(r,\theta) - D_n'(r,\theta)\cot\theta_2, \quad \text{(C34)}$$

where P_n is the Legendre polynomial of order *n*.

For the slow translation of a soft spherical particle inside a concentric spherical cavity ($d = 0$), the exact solution of its drag force in Eq. (B16) was obtained explicitly with (Keh and Chou 2004)

$$D_{22} = 6\frac{U\gamma}{\lambda\Delta}[60\alpha\beta^2 - (2\beta^4 s_5 - 3\alpha^2 s_6 + \alpha\beta s_0 s_7)\cosh(\beta-\alpha)$$
$$+ (2\beta^3 s_8 + \alpha s_0 s_6 - 3\alpha^2\beta s_7)\sinh(\beta-\alpha)], \quad \text{(C35)}$$

where

$$\Delta = 12\alpha s_{22} + (9\alpha^2 s_{19} - \alpha s_0 s_{20} - 2\beta s_{21})\cosh(\beta-\alpha)$$
$$+3(2s_{23} + \alpha s_0 s_{19} - \alpha^2 s_{20})\sinh(\beta-\alpha); \quad \text{(C36)}$$

$$s_0 = \alpha^2 + 3, \qquad s_5 = \beta^5 + 15\beta^3 - \gamma^5, \qquad s_6 = 6\beta^5 + 45\beta^3 - \gamma^5,$$

$$s_7 = \beta^5 + 45\beta^3 - \gamma^5, \qquad s_8 = 6\beta^5 + 15\beta^3 - \gamma^5,$$

$$s_{19} = 8\beta^5 - 15\beta^4\gamma + 60\beta^3 + 10\beta^2\gamma^3 - 3\gamma^5,$$

$$s_{20} = 4\beta^6 - 9\beta^5\gamma + 180\beta^4 + 10\beta^3\gamma(\gamma^2 - 18) - 9\beta\gamma^5 + 4\gamma^6,$$

$$s_{21} = 4\beta^8 - 9\beta^7\gamma + 60\beta^6 + 2\beta^5\gamma(5\gamma^2 - 63) - 3\beta^3\gamma(3\gamma^4 - 20\gamma^2 + 90) + 4\beta^2\gamma^6 + 6\gamma^6,$$

doi:10.6342/NTU202502609

$$s_{22} = 20\beta^6 - 27\beta^5\gamma + 5\beta^3\gamma(\gamma^2 - 18) + 2\gamma^6,$$

$$s_{23} = 8\beta^8 - 15\beta^7\gamma + 20\beta^6 + 2\beta^5\gamma(5\gamma^2 - 36) - \beta^3\gamma(3\gamma^4 - 20\gamma^2 + 90) + 2\gamma^6, \quad \text{(C37)}$$

$\alpha = \lambda a$, $\beta = \lambda b$, and $\gamma = \lambda c$.

doi:10.6342/NTU202502609